ADVANCED MATERIALS
www.advmat.de

Development of Bioorthogonally Degradable Tough Hydrogels Using Enamine *N*-Oxide Based Crosslinkers

*Thomas T. Kim, Deep Malu, Dongjing He, Yuhang Hu, and Justin Kim**

Inducibly degradable polymers present new opportunities to integrate tough hydrogels into a wide range of biomaterials. Rapid and inducible degradation enables fast transition in material properties without sacrificing material integrity prior to removal. In pursuit of bioorthogonal chemical modalities that will enable inducible polymer degradation in biologically relevant environments, enamine *N*-oxide crosslinkers are developed for double network acrylamide-based polymer/alginate hydrogels. Bioorthogonal dissociation initiated by the application of aqueous diboron solution through several delivery mechanisms effectively lead to polymer degradation. Their degradation by aqueous $B_2(OH)_4$ solution results in a fracture energy half-life of <10 min. The biocompatibility of the degradable hydrogels and $B_2(OH)_4$ reagent is assessed, and the removability of strongly adhered tough hydrogels on mice skin is evaluated. Thermoresponsive PNiPAAm/Alg hydrogels are fabricated and application of the hydrogels as a chemically inducible degradable intraoral wound dressing is demonstrated. It is demonstrated through in vivo maximum tolerated dose studies that diboron solution administered to mice by oral gavage is well tolerated. Successful integration of enamine *N*-oxides within the tough double network hydrogels as chemically degradable motifs demonstrates the applicability of enamine *N*-oxides in the realm of polymer chemistry and highlights the importance of chemically induced bioorthogonal dissociation reactions for materials science.

1. Introduction

Hydrogels, hydrophilic polymer networks that can absorb and retain high volumes of water,[1] have been identified as ideal biomaterials due to their high water content, tunable physical and chemical properties,[2,3] and biocompatibility. As a result, hydrogels have seen many uses in biomedical applications such as biomedical devices,[4,5] drug delivery systems,[6–8] and tissue engineering.[9–11] Despite the hydrogel's ability to possess similar water content to native biological tissues, most exhibit poor material toughness, limiting their use in load-bearing and mechanically deforming biomedical settings.[12] In efforts to improve the hydrogel's mechanical properties, new approaches have been developed to enhance the toughness of hydrogels, including double network (DN) hydrogels,[13–15] nanocomposite hydrogels,[16,17] and slide-ring hydrogels.[18]

Notably, the ease of preparation and the tunable nature of DN hydrogels have gained significant attention in recent years.[19] These hydrogels combine two independently crosslinked polymers to create an interpenetrating network that works synergistically to dissipate energy and resist fracture. For example, DN hydrogels of poly(acrylamides) (PAAm) covalently crosslinked with bisacrylamides, and alginates (Alg) physically crosslinked with divalent cations have been reported to be capable of stretching >20 times their initial length with fracture energies >6 kJ m^{-2}.[14] As a result, the enhanced toughness of hydrogels has expanded their applications to tough hydrogel adhesives,[20] cartilage repair,[21,22] soft robotics,[23–25] contact lenses,[26,27] wound dressings,[28–30] and other areas where both durability and flexibility are essential.

T. T. Kim, J. Kim
School of Chemistry and Biochemistry
Georgia Institute of Technology
Atlanta, GA 30332, USA
E-mail: jkim4172@gatech.edu

The ORCID identification number(s) for the author(s) of this article can be found under https://doi.org/10.1002/adma.202414692

DOI: 10.1002/adma.202414692

T. T. Kim, J. Kim
Department of Cancer Biology
Dana-Farber Cancer Institute
Boston, MA 02215, USA

T. T. Kim, J. Kim
Department of Biological Chemistry and Molecular Pharmacology
Harvard Medical School
Boston, MA 02115, USA

D. Malu, D. He, Y. Hu
George W. Woodruff School of Mechanical Engineering
Georgia Institute of Technology
Atlanta, GA 30332, USA

D. Malu, D. He, Y. Hu
School of Chemical and Biomolecular Engineering
Georgia Institute of Technology
Atlanta, GA 30332, USA

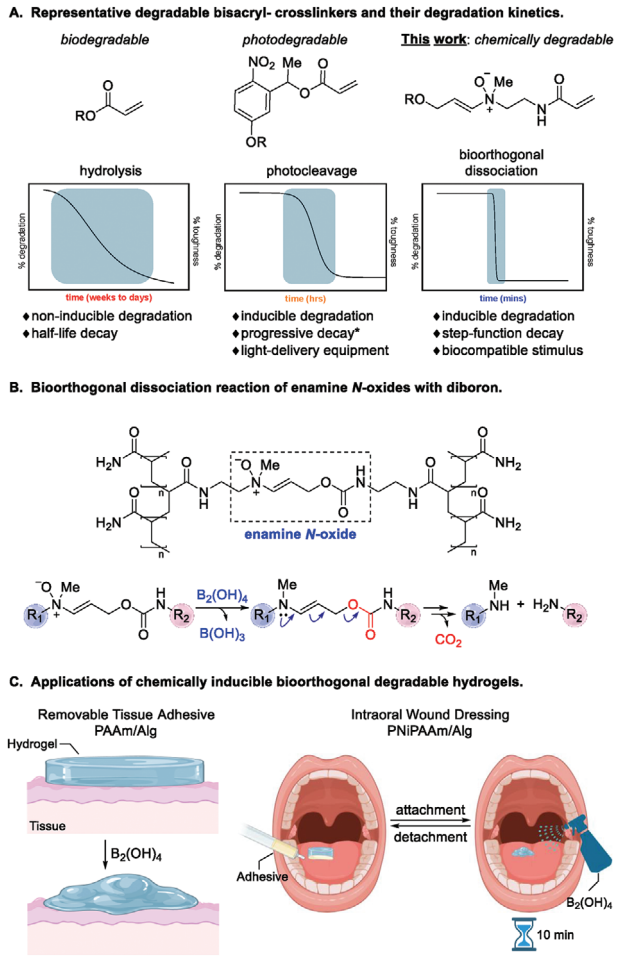

Figure 1. Degradable bisacrylamide/acrylate chemical crosslinkers. A) Molecular structures of degradable functional groups of chemical crosslinkers and relative degradation profiles of hydrogels cast with degradable crosslinkers. *Certain photodegradable hydrogel applications exhibit a degradation timescale of minutes.[59] B) Bioorthogonal dissociation reaction of polyacrylamides crosslinked with enamine *N*-oxide and diboron reagent in aqueous solution. C) Degradable PAAm/Alg hydrogel's application as removal tissue adhesives and degradable PNiPAAm/Alg hydrogel's application as removal intraoral wound dressings.

However, the superior toughness and adhesive strengths of DN hydrogels have spawned a new challenge: their removal. Leaving materials in place beyond their serviceable lifetime risks long-term adverse effects. Yet, their removal risks secondary tissue damage,[31] fibrosis,[32] and may involve invasive surgical interventions.[33] Degradable systems provide an effective solution to this challenge.

There are two distinct classes of degradable biomaterials, each with its own set of design philosophies and applications: biodegradable materials and inducibly degradable materials. Biodegradable materials undergo degradation via environmental factors (e.g., enzymatic digestion,[34–36] hydrolysis,[8,37–39] oxidation)[40–42] and exhibit decay with a characteristic half-life during and beyond their serviceable lifetime (**Figure 1A**). These materials have seen applications in areas such as implantable hydrogel devices,[43,44] tissue engineering,[45,46] and drug delivery systems.[47,48] On the other hand, inducibly degradable materials maintain their structural or functional integrity while in service but rely on external stimuli to trigger degradation, offering a sharper transition in material properties. This report concerns the latter.

Stimuli-responsive soft materials featuring a wide range of triggers such as heat,[49,50] pH,[51] magnetism,[52,53] and light[54,55] have been described previously with photodegradable hydrogels featuring prominently. These materials find applications in biosensors,[56] vascular grafts,[57,58] and ingestible medical devices;[59] however, opportunities exist for further advances in this space. Materials featuring faster degradation kinetics, greater biocompatibility, minimal invasiveness, improved degradation scope, and broader accessibility are desired, and designing several if not all these aspects into a material is the aspiration. For instance, photoresponsive gels offer some of the fastest degradation kinetics, but with few exceptions of precisely engineered devices that place a light source directly adjacent to a hydrogel target,[59] light-inducible methods generally achieve degradation of PAAm/Alg hydrogels on the order of 2–24 h depending on the light source and placement as well as material size and composition.[60] Light-based degradation strategies are unrivaled in spatial precision but are likewise challenged by substrates with large, diffuse, or amorphous geometries. Issues of tissue penetration, accessibility of an appropriate light source, and invasiveness of endoscopic procedures needed for the degradation of internally implanted hydrogels are additional points of concern.

Here, we introduce a new modality for rapid polymer degradation employing a bioorthogonal chemical reaction (Figure 1B). The reaction is rapid, and its components are flexible in delivery, readily accessible, highly biocompatible, and can be substituted for their non-degradable counterpart in hydrogels without significant loss of performance. We demonstrate these features in applications of tough double network PAAm/Alg hydrogels and extend the work to oral wound dressings using a non-swelling poly(*N*-isopropylacrylamide) (PNiPAAm)/Alg variant (Figure 1C). Bioorthogonal reagent-induced degradation offers opportunities in applications where a material's service lifetime is very short, such as in wound dressings requiring frequent attachment and removal or where a temporary device is installed but requires undiminished performance over an extended period of time.

2. Results and Discussion

This work leverages the bioorthogonal dissociation reaction between enamine *N*-oxide and diboron reagents. We previously reported that enamine *N*-oxides undergo hypoxia-dependent reduction and fragmentation in the presence of hemeproteins to activate a caged prodrug and a latent electrophile.[61] We also described how the biological trigger could be substituted with a chemical trigger to induce enamine *N*-oxide fragmentation. Specifically, we found diboron could initiate bioorthogonal bond cleavage between protein and small molecule.[62] We now demonstrate that the enamine *N*-oxide motif can be used to engineer biocompatible materials whose polymeric network can be decrosslinked by a diboron chemical trigger.

Degradation of tough double network PAAm/Alg hydrogels can be achieved by disrupting either its physical or covalent

crosslinks; Mooney and co-workers have shown that disruption of a single network is sufficient to significantly degrade performance.[39] The physical crosslinks were targeted by Kobašlija and McQuade using the metal cation chelating agent ethylenediaminetetraacetic acid (EDTA)[63] while the covalent crosslinks were targeted by Mooney and co-workers in enzyme or hydrolysis-dependent biodegradable materials.[39] In this work, we focused on disrupting the latter with the goal of achieving a sharper degradation profile than the 2 week to several month half-lives achieved by such biodegradable systems.

The typical nondegradable tough hydrogel was converted to a degradable tough hydrogel by replacing the non-degradable acrylate functionalized crosslinker (*N,N'*-methylenebis(acrylamide), MBAA) with the inducibly degradable analog enamine *N*-oxide bis(acrylamide) (ENBAA).

2.1. Synthesis of ENBAA Crosslinkers

Enamine *N*-oxides can be synthesized by intermolecular retro-Cope elimination reaction between hydroxylamines and alkynes;[61] however, we anticipated that the regioselectivities achieved through this reaction would be insufficient for the current application. In instances where complete polymer decrosslinking is desired for thorough material degradation, exclusive formation of enamine *N*-oxides with the anti-Markovnikov regiochemistry was deemed to be paramount. Unlike its counterpart, the regioisomeric Markovnikov addition product does not undergo rapid fragmentation upon treatment with aqueous diboron reagents under equivalent conditions. While the regioselectivity of the hydroamination reaction is strongly governed by propargylic substituent inductive effects on the alkyne component and judicious choice of such substituents is known to improve regioselectivity in some applications,[64] here, the composition of the alkyne is constrained by the need for a propargylic carbamate at the propargylic position where it serves as both a convenient linkage and a superb leaving group. Unfortunately, hydroamination of propargylic carbamates does not produce enamine *N*-oxides with regioisomeric purity.

Scheme 1A describes the first-generation route to bisacrylamide enamine *N*-oxide crosslinkers. Hydroamination of alkyne **2** featuring a propargylic carbamate with hydroxylamine **1** resulted in formation of an 8.3:1 ratio of regioisomers favoring the desired anti-Markovnikov product **3** over the undesired Markovnikov product **4**. Notably, the regioisomers were inseparable by both standard flash column chromatography and reverse phase high-performance liquid chromatography (HPLC). Reduction of each with an aqueous solution of tetrahydroxydiboron ($B_2(OH)_4$) reagent resulted in reductive fragmentation of the former to amines **5** and **6** and the latter to enamine **7**, poignantly highlighting the challenges of advancing a regioisomeric mixture.

Alternatively, prior studies demonstrated that terminally halogenated alkynes undergo rapid and regioselective hydroamination with *N,N*-dialkylhydroxylamines to produce regioisomerically pure enamine *N*-oxides with the anti-Markovnikov constitution.[64,65] While it was determined that *α*-haloenamine *N*-oxides featuring a primary carbamate at the allylic position cannot be directly employed for polymer degradation as currently designed since their reductive activation does not lead to complete and rapid dissociation, we posited that dehalogenation would afford the enamine *N*-oxide crosslinker precursor **3** that we originally targeted.

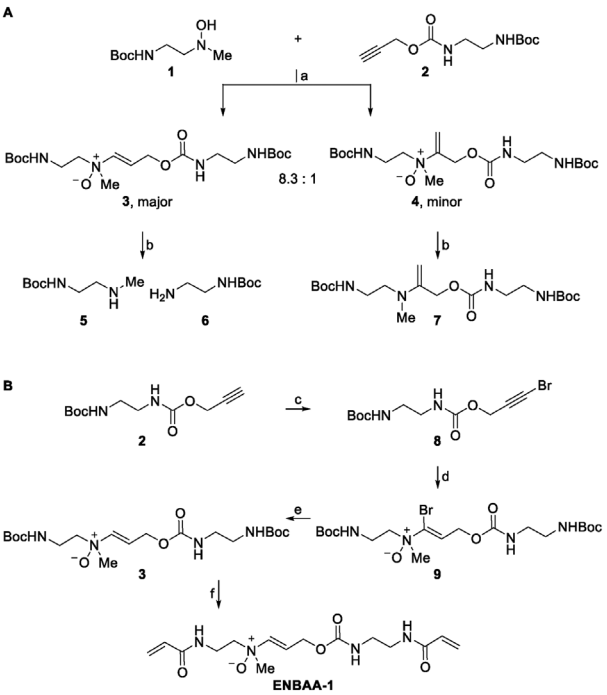

Scheme 1. Synthesis of enamine *N*-oxide-based bioorthogonally degradable bisacrylamide crosslinkers. Reagents and conditions: a) Hydroxylamine **1** (2 equiv), alkyne **2** (1 equiv), 20% TFE/$CHCl_3$ (v/v), 60 °C, 56%, b) $B_2(OH)_4$, H_2O, c) NBS, $AgNO_3$, acetone, 0 °C, 91%, d) **1** (2 equiv), 20% TFE/$CHCl_3$ (v/v), 50 °C, 92%, e) *n*BuLi, THF, −78 °C; H_2O, 23 °C, 76%, f) 20% TFA/CH_2Cl_2 (v/v), 23 °C; *N*-acryloxysuccinimide, $NaHCO_3$, H_2O, 23 °C, 80% (2-step). TFE, 2,2,2-trifluoroethanol; NBS, *N*-bromosuccinimide; THF, tetrahydrofuran; TFA, trifluoroacetic acid.

Scheme 1B describes the efficient regioselective synthesis of enamine *N*-oxide bisacrylamide (ENBAA) crosslinkers. Retro-Cope elimination reaction between hydroxylamine **1** and bromoalkyne **8** yielded bromoenamine *N*-oxide **9** in 92% yield as a single regioisomer. Subsequent lithium-bromine exchange using *n*-BuLi followed by protonation of the vinyllithium intermediate with water afforded enamine *N*-oxide **3**. Then, Boc-deprotection followed by acryloylation using *N*-acryloxysuccinimide in basic aqueous solution afforded enamine *N*-oxide bisacrylamide ENBAA-1 in 80% yield over two steps. To synthesize crosslinkers of varying lengths, hydroxylamines **S8** and **S9** were employed in the hydroamination reaction with bromoalkyne **8**. These ENBAA crosslinkers were then used to fabricate PAAm/Alg hydrogels.

2.2. ENBAA Linker Length Study and Fabrication of Degradable Tough Hydrogel

To fabricate PAAm/Alg hydrogels, high and low molecular weight sodium alginates were physically crosslinked using calcium sulfate. Acrylamides were covalently crosslinked using either nondegradable MBAA or degradable enamine *N*-oxide bisacrylamides (ENBAA) 1–3 (**Figure** 2A).

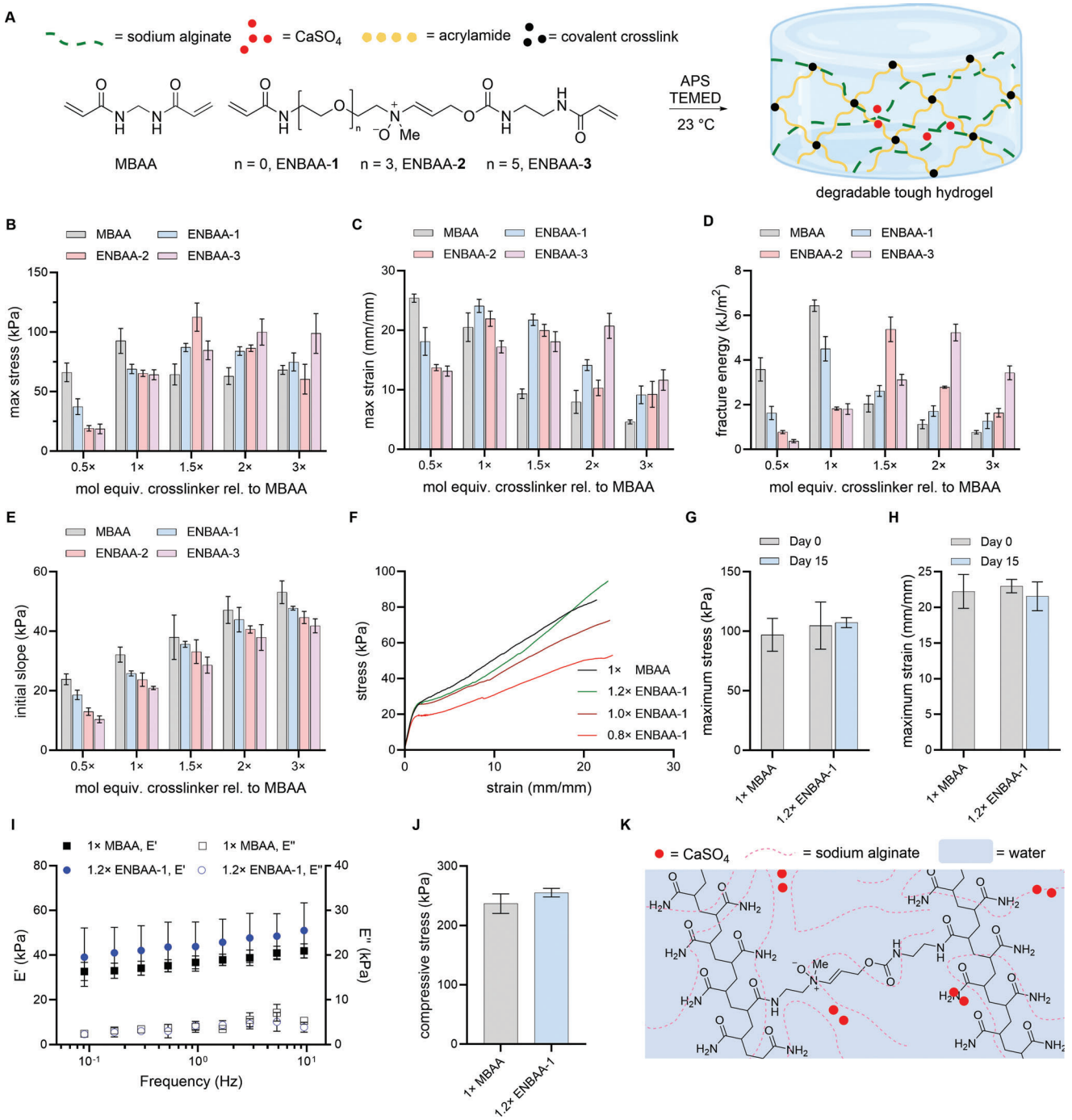

Figure 2. Fabrication and mechanical properties of degradable double network PAAm/Alg hydrogels using crosslinkers ENBAA-1–3. A) Illustration highlighting monomers, crosslinkers, and polymerization reagents used to fabricate degradable PAAm/Alg hydrogels. The effect of crosslinker length on the B) maximum stresses, C) maximum strains, D) fracture energies, and E) initial slopes of the stress-strain curves in the strain range of 0–1 mm mm^{-2} of PAAm/Alg hydrogels fabricated with varying covalent crosslinker concentrations (MBAA, ENBAA-1–3) measured under tensile loading. Mean values are shown, and error bars represent ± SD ($n = 3$). F) Stress-strain curves comparing PAAm/Alg hydrogels cast with MBAA and varying concentrations of ENBAA-1 crosslinker relative to that of MBAA. The maximum G) stress and H) strain of PAAm/Alg hydrogels cast with ENBAA-1 crosslinker and stored at 37 °C for 15 d are plotted. Mean values are shown, and error bars represent ± SD ($n = 3$). I) Viscoelastic responses of PAAm/Alg hydrogels cast with MBAA and ENBAA-1 crosslinkers measured by dynamic mechanical analysis (DMA). Mean values are shown, and error bars represent ± SD, ($n = 3$). J) Compressive stresses at 80% strain of PAAm/Alg hydrogels cast with MBAA and ENBAA-1 crosslinkers measured under compressive loading. Mean values are shown, and error bars represent ± SD ($n = 3$). K) Illustration of PAAm/Alg hydrogels crosslinked with ENBAA-1 crosslinker.

To evaluate the effect of the covalent crosslinker length on the mechanical properties of PAAm/Alg hydrogels, crosslinkers ENBAA-1–3 were used to fabricate the hydrogels (Table S1, Supporting Information). Stress–strain curves were obtained under tensile loading, and the maximum stress and strain, fracture energies, and the initial slope of the stress-strain curve were compared (Figure 2B–E; Figures S1–S4, Supporting Information). Fracture energies were determined using a method introduced by Rivlin.[66] Nondegradable hydrogels fabricated with MBAA crosslinkers have been reported to give a maximum stress of 156 kPa, maximum strain of >20 mm/mm, and a fracture energy of >6 kJ m^{-2}.[14] Our goal was to find an enamine *N*-oxide crosslinker that would perform similarly to the MBAA crosslinker while using the least amount of the crosslinker. This would enable the use of lower effective concentrations of the chemical inducer. Linker length studies revealed that as the covalent crosslinker length increases, greater stoichiometries of the crosslinkers are necessary to obtain a similar stress, strain, fracture energy, and the initial slope of the stress-strain curve. When comparing the fracture energies of hydrogels made with different crosslinkers, hydrogels made with ENBAA-1 at 1× mol equivalent relative to MBAA had fracture energies that were twice as large as those of hydrogels made with ENBAA-3 at 1× mol equivalent relative to MBAA. Moreover, hydrogels cast with ENBAA-3 required more than 2× the amount of crosslinkers to obtain similar mechanical properties compared to those cast with MBAA. These trends have been reported previously. As the covalent crosslinker lengths increase, greater stoichiometries of the crosslinker is necessary to achieve comparable mechanical properties.[39,67,68]

Because the intrinsic physicochemical properties of the enamine *N*-oxide crosslinkers are different from those of MBAA, it was essential to optimize the relative amount of the crosslinker to obtain hydrogels with mechanical properties comparable to those of the nondegradable tough hydrogels. We observed that hydrogels cast with 1.2× ENBAA-1 crosslinkers behaved most like those cast with MBAA (Figure 2F; Figure S5, Supporting Information). Moreover, degradable tough hydrogels maintained their mechanical properties even after incubation at 37 °C for 15 d (Figure 2G,H; Figure S6, Supporting Information), highlighting the stability of enamine *N*-oxide crosslinkers under physiologically relevant conditions for extended periods of time. Viscoelastic responses measured by dynamic mechanical analysis (DMA) and compressive stresses of hydrogels further confirm the similar mechanical properties between the nondegradable and degradable tough hydrogels (Figure 2I,J; Figure S7, Supporting Information). Figure 2K depicts PAAm/Alg hydrogels cast with covalent crosslinker ENBAA-1.

2.3. Degradation of PAAm/Alg Tough Hydrogels

Next, we evaluated the degradation of hydrogels fabricated with enamine *N*-oxide crosslinkers starting with the degradation of PAAm hydrogels incorporating crosslinker ENBAA-1 (Figure S8, Supporting Information). Previously, we reported the second-order rate constant for the reductive dissociation of enamine *N*-oxides by diboron reagents in solution phase to be 82 $M^{-1}s^{-1}$.[62] To evaluate the degradation of PAAm hydrogels with $B_2(OH)_4$, PAAm hydrogels were exposed to 10 mM aq. $B_2(OH)_4$, and complete dissolution of the hydrogel was observed within 20 min by vial inversion tests.

We also demonstrated the diboron-induced degradation of tough DN PAAm/Alg hydrogels. PAAm/Alg hydrogels cast with blue food coloring were exposed to 500 μM aq. $B_2(OH)_4$, and we observed that these gels were degraded considerably within 20 min (**Figure 3**A; Figure S9, Supporting Information). The mechanical properties of hydrogels exposed to $B_2(OH)_4$ were evaluated further by obtaining their stress-strain curves (Figure 3B–E). We observed significant degradation of the hydrogels even when they were exposed to 500 μM aq. $B_2(OH)_4$ for 10 min with a decrease in maximum stress from 90 to 18 kPa, and fracture energy from 6.8 to 0.3 kJ m^{-2}. Hydrogels exposed to $B_2(OH)_4$ for 3 and 20 min have also been evaluated (Figures S10 and S11, Supporting Information).

Photos of PAAm/Alg hydrogels exposed to 500 μM aq. $B_2(OH)_4$ for 10 min then placed under tension are displayed in Figure 3F. Diboron induced degradation of the PAAm/Alg hydrogels are apparent. The gels have clearly lost most of their mechanical properties as evidenced by formation of holes in the middle of the gel even at low strain. Surprisingly, the mechanical properties remained largely intact for hydrogels exposed to 100 μM aq. $B_2(OH)_4$. Although we observed a greater than twofold decrease in fracture energy, the maximum stress was maintained at 80 kPa at >35 mm mm^{-1} strain. The increase in strain and a decrease in the initial slopes of the stress-strain curves are both reflected in the stress-strain curves, which suggests that only partial degradation has occurred despite the excess amount of $B_2(OH)_4$ used relative to the crosslinker.

To determine whether the marginal degradation was due to poor diffusion of the diboron solution into the hydrogel, the degradation of 1.5 and 1.0 mm thick PAAm/Alg hydrogels were evaluated at varying concentrations of $B_2(OH)_4$ (**Figure 4**A–D; Figure S12, Supporting Information). 1.0 mm thick hydrogels reacted with $B_2(OH)_4$ more effectively across all concentrations. The greatest difference was observed at 100 μM $B_2(OH)_4$ where the maximum stress decreased below 20 kPa and the fracture energy decreased to less than 1 kJ m^{-2} for 1.0 mm thick gels.

To better understand the effect of gel thickness on the rate of degradation, the hydrogels' (1.0 or 1.5 mm thick, 5 mm diameter) shear moduli were measured in the presence of aqueous $B_2(OH)_4$ (Figure 4E,F; Figure S13, Supporting Information). Discrete rheology measurements of hydrogels exposed to $B_2(OH)_4$ with concentrations ranging from 100 μM to 10 mM show that 1.0 mm thick gels respond to $B_2(OH)_4$ faster across all concentrations. At 500 μM [$B_2(OH)_4$], a 10-fold decrease in G' was achieved by 45 min. To better visualize the relative trends between samples, the fraction storage modulus was calculated and plotted by normalizing the modulus with the initial storage modulus (Figure 4G; Figure S14, Supporting Information). Expectedly, 1.0 mm thick gels responded to $B_2(OH)_4$ across all concentrations. Even for 100 μM and 500 μM concentrations of aq. $B_2(OH)_4$ tested, the storage moduli of both 1.0 and 1.5 mm thick gels all decreased by more than half in less than 10 min. Tensile testing data coupled with viscoelastic responses of hydrogels with these dimensions and geometry strongly suggest that PAAm/Alg hydrogels fabricated with ENBAA-1 as the chemical crosslinker can undergo induced degradation using $B_2(OH)_4$ within 10 min. Moreover, the data indicate that the rate of degradation is limited by the rate

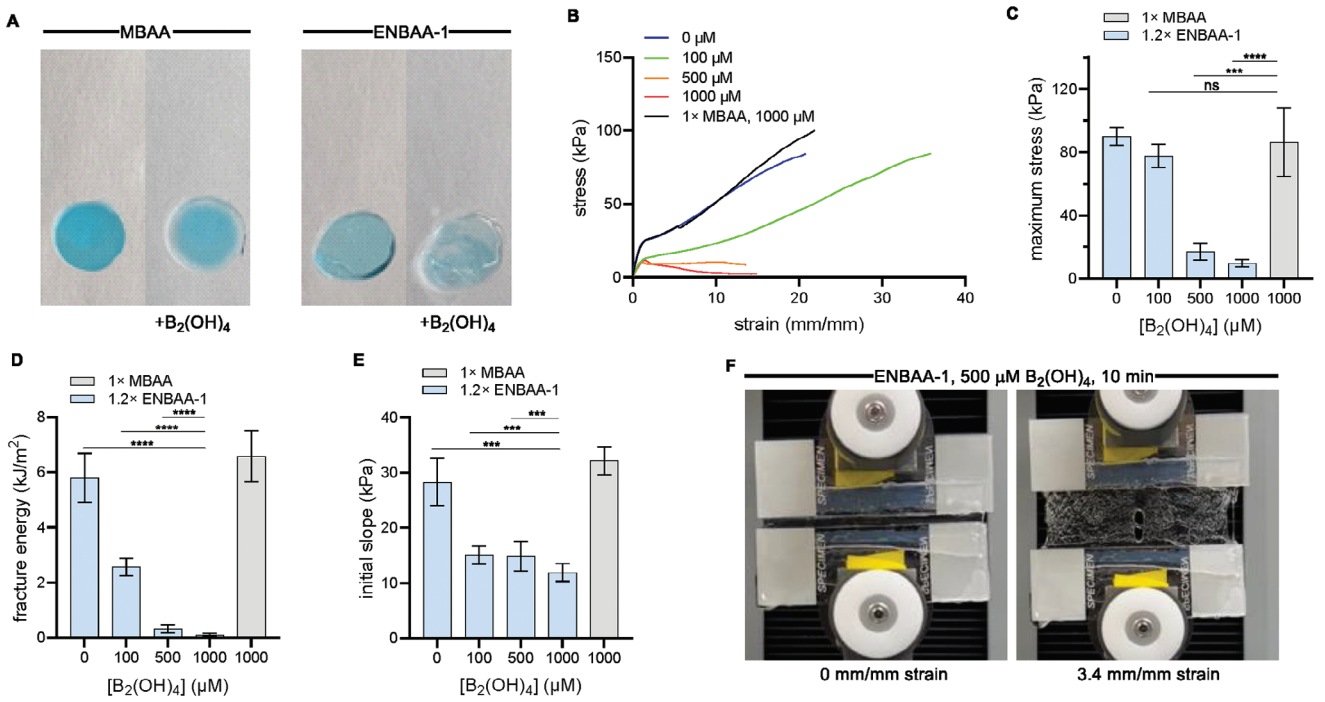

Figure 3. Degradation profiles of degradable 1.5 mm thick PAAm/Alg hydrogels. A) Photos of PAAm/Alg hydrogels before and after exposure to aqueous $B_2(OH)_4$ (500 μM) for 20 min. Degradation of PAAm/Alg hydrogels cast with ENBAA-1 crosslinkers evaluated by tensile tests. B) Stress–strain curves, C) maximum stresses, D) fracture energies, and E) initial slopes of the stress-strain curves in the strain range of 0–1 mm mm^{-2} of PAAm/Alg hydrogels exposed to various concentrations of aqueous $B_2(OH)_4$ for 10 min. F) Photos of PAAm/Alg hydrogels exposed to aqueous $B_2(OH)_4$ (500 μM) for 10 min under tensile loading. Before tensile pull (left) and at 3.4 mm mm^{-1} strain (right). Mean values are shown, and error bars represents ± SD ($n = 3$). Statistical analysis by a one-way ANOVA with post hoc *t*-tests with Bonferroni correction, ****$p < 0.0001$, ***$p < 0.001$, ns = no significance between groups.

of diffusion of the diboron solution into the hydrogel for gels with these dimensions and geometry.

2.4. Biocompatibility and Removability of Degradable Tough Hydrogels

To assess the biocompatibility of the PAAm/Alg hydrogels, the gels were placed on top of a monolayer of L929 fibroblast cells in tissue culture. After incubation for 72 h, the gels were degraded with 500 μM aq. $B_2(OH)_4$ then stained with Calcein AM and ethidium homodimer 1 (**Figure 5A**). The cells were imaged with a fluorescence microscope, showing live and dead cells (Figure 5B). The cell viability was calculated for cells treated with or without the degradable hydrogel, and the results showed no statistical differences between the two groups (Figure 5C). Similarly, the cytotoxicity of $B_2(OH)_4$ was also evaluated on L929 cells. L929 cells were treated with $B_2(OH)_4$ at concentrations up to 50 mM, incubated for 0.5 or 3 h, then assayed by the CellTiter-Glo cell viability assay. Cells treated with diboron for 0.5 h showed an IC_{50} value of >20 mM, and cells treated with diboron for 3 h showed an IC_{50} value of >9 mM, both well above the concentrations and exposure times required to effectively degrade the PAAm/Alg hydrogels (Figure 5D).

With a bioorthogonal means of degrading hydrogels in hand, we looked to evaluate the gels as adhesives, which are an important application of tough hydrogels. The ability of ENBAA-crosslinked degradable tough hydrogels to adhere to porcine skin was evaluated by T-peel test using three adhesives: 1) chitosan with EDC and sulfo-NHS, 2) commercially available gel-type cyanoacrylate adhesive Loctite 4541, and 3) commercially available high viscosity liquid-type cyanoacrylate adhesive Periacryl 90HV (**Figure 6A**). While many types of chitosan adhesives have been reported in the literature, including covalent adhesives based on chitosan solution supplemented with EDC and sulfo-NHS,[20] pH-responsive topological adhesives based on chitosan adsorbed on a dissipative matrix,[69] or chitosan-based films,[70] we chose chitosan adhesives supplemented with EDC and sulfo-NHS.

Adhesion energies were determined by taking twice the plateau value of the ratio of the force to width.[66] Of the three adhesives tested, chitosan + EDC/sulfo-NHS proved to be the most effective adhesive with an adhesion energy of 710 J m^{-2}, followed by Periacryl with 550 J m^{-2}, then Loctite with 290 J m^{-2}. Moreover, when comparing the adhesion energies of nondegradable and inducibly degradable hydrogels on porcine skin, no significant differences were observed (Figure 6B).

Using our inducibly degradable gels, we confirmed that chitosan acts as a strong adhesive even on wet surfaces and that the adhesion energies are not compromised in the presence of blood as previously reported.[20] In contrast, the cyanoacrylate-based adhesives Loctite and Periacryl exhibited poor adhesion

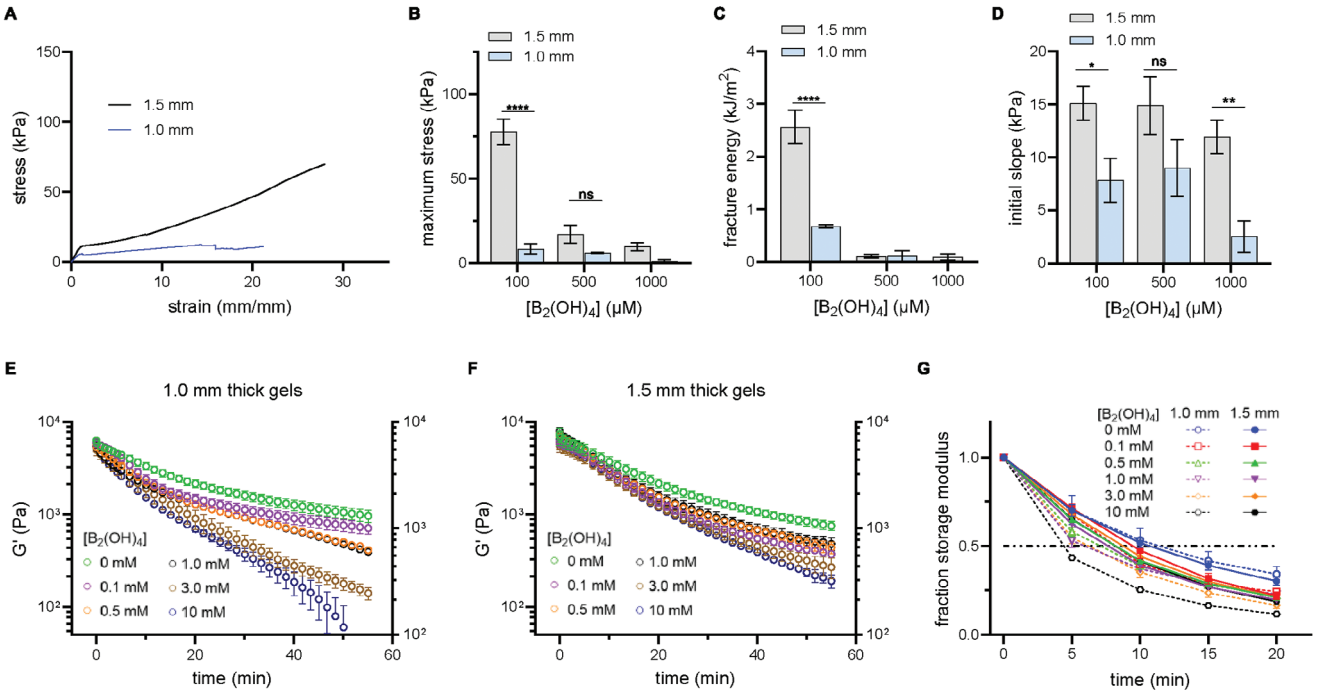

Figure 4. Degradation profiles of 1.0 and 1.5 mm thick PAAm/Alg hydrogels evaluated with tensile and rheology tests. A) Stress–strain curves, B) maximum stresses, C) fracture energies, and D) initial slopes of the stress-strain curves in the strain range of 0–1 mm mm^{-2} of PAAm/Alg hydrogels of varying thickness exposed to various concentrations of aqueous $B_2(OH)_4$ for 10 min. Mean values are shown, and error bars represents ± SD ($n = 3$). E) Shear storage moduli of 1.0 mm thick, and F) 1.5 mm thick PAAm/Alg hydrogels cast with ENBAA-1 exposed to aqueous $B_2(OH)_4$. Mean values are shown, and error bars represents ± SD ($n = 3$). G) Fraction storage modulus of 1.0 and 1.5 mm thick PAAm/Alg hydrogels cast with ENBAA-1 exposed to aqueous $B_2(OH)_4$. Mean values are shown, and error bars represents ± SD ($n = 3$). Statistical analysis by a one-way ANOVA with post hoc *t*-tests with Bonferroni correction, ****$p < 0.0001$, **$p < 0.01$, *$p < 0.05$, ns = no significance between groups.

energies when blood was applied to the surface of tissues prior to adhesion (Figure S15, Supporting Information). This is consistent with the known incompatibility of cyanoacrylate adhesives with wet surfaces. Both adhesives solidify immediately upon exposure to water and form plastics that cannot accommodate dynamic movements of the tissues.

Strong adhesion energies are important for holding a material in place; however, they can be a problem when detachment is required. For example, the removal of strong adhesives from various tissues risks fibrosis and other forms of secondary tissue damage. An effective approach to this challenge is to degrade the underlying biomaterial to which the adhesive has been applied. When a material's mechanical properties are compromised, its ability to adhere also decreases as the toughness of a material is linked to the strength of its adhesion to biological tissues, and the two cannot be decoupled.[39,71] To evaluate the effect of hydrogel degradation on the adhesion energies, hydrogels were adhered to mice skin then removed with or without degradation. The tissues were then stained and assessed by histology (Figure 6C; S16, Supporting Information). Removal of both MBAA and ENBAA-1 crosslinked PAAm/Alg hydrogels from mice skin without degradation resulted in the detachment of the outer layer of epithelium when adhesives such as Periacryl and chitosan were used; however, the epithelia were observed to be intact when the hydrogels were peeled after submerging the tissue in an aqueous solution of 500 μM $B_2(OH)_4$ for 30 min.

3. Poly(*N*-isopropylacrylamide)/Alginate Intraoral Hydrogels in Wet Environments

PAAm/Alg hydrogels are tough and powerful in dry environments. However, once introduced to a wet environment where the hydrogel can absorb the solvent, PAAm/Alg hydrogels' toughness decreases due to swelling.[72] To minimize the effect that swelling has on the intrinsic properties of the material, degradable thermoresponsive poly(*N*-isopropylacrylamide) (PNiPAAm)/Alg hydrogels were also fabricated using the same ENBAA-1 crosslinker. PNiPAAms undergo phase transition above its low critical solution temperature (LCST) which allows for de-swelling, maintaining the material's original mechanical properties.[73,74] And because PNiPAAm's LCST is below 37 °C or the normal body temperature, PNiPAAm/Alg hydrogels are suitable for applications in vivo under wet environments.[75–77] Developing a robust, biocompatible, and chemically inducible tough hydrogel could enable the use of these materials in a range of in vivo applications, where repeated detachment is crucial.

Tough degradable hydrogel wound dressings are most attractive in applications where the surrounding environment undergoes consistent deformations and where repeated attachment and detachment is favorable. The intraoral cavity is one organ where hydrogel wound dressings can have an impact (**Figure** 7A). Attachment of tough hydrogels to oral lesions such as mouth ulcers, sores, or post-surgical sutures can be beneficial to protect the site of injury from food or beverage as well as from

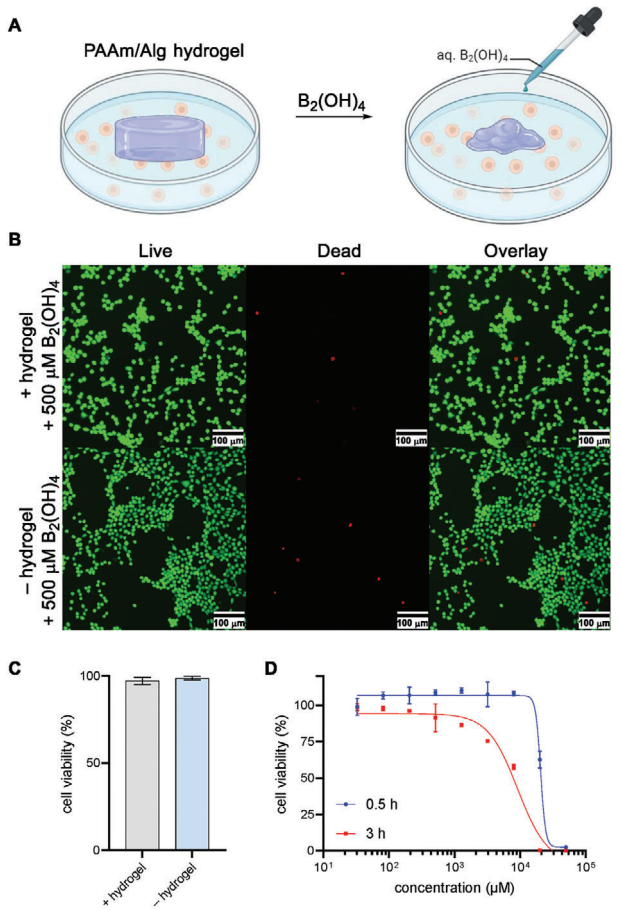

Figure 5. Biocompatibility of degradable PAAm/Alg hydrogel and $B_2(OH)_4$ reagent. A) Illustration of the biocompatibility assay of PAAm/Alg hydrogels. B) Fluorescence microscope images of cells stained with Calcein AM (left, green), ethidium homodimer-1 (middle, red), and overlay of two channels (right). C) Cell viability of L929 cells incubated with PAAm/Alg hydrogels and exposed to aqueous $B_2(OH)_4$ (500 μM) for 30 min at 37 °C. Cell viability was calculated using a custom pipeline on CellProfiler. Mean values are shown, and error bars represents ± SD (n = 5). D) L929 fibroblasts exposed to $B_2(OH)_4$ were evaluated for cell viability using the CellTiter-Glo 2.0 assay. Mean values are shown, and error bars represents ± SD (n = 3).

secondary infections;[78,79] however, because the intraoral cavity is constantly wet from saliva, hydrogels that undergo extreme swelling are not ideal materials for oral wound dressings. For example, PAAm/Alg hydrogels undergo significant swelling when immersed in water.[80] Many anti-swelling and adhesive hydrogels have been developed to address the swelling behaviors of hydrogels.[78,81] To create tough hydrogels that can maintain their mechanical properties in wet environments at biological temperatures, we turned our attention to PNiPAAm/Alg hydrogels. PNiPAAms are well known for their thermo-responsive characteristics and PNiPAAm/Alg hydrogels have been reported for applications in drug delivery and soft robotics.[82,83]

To evaluate the swelling of PAAm/Alg and PNiPAAm/Alg hydrogels in various aqueous media, the swelling ratios for these hydrogels were measured (Figure 7B). Hydrogels were immersed in PBS, pH 7.4 at either 23 or 37 °C for 72 h, and the swelling ratios were recorded. At room temperature, both PAAm/Alg and PNiPAAm/Alg hydrogels showed swelling ratios up to 40-fold. At 37 °C, although PAAm/Alg hydrogels showed similar final swelling ratios, PNiPAAm/Alg hydrogels showed deswelling from the originally fabricated state, with a swelling ratio of 0.6-fold. This data is consistent with other PNiPAAm-based hydrogels that are swelled above their LCST. The *N*-isopropyl groups interfere with hydrogen bonding and causes deswelling. Photos of hydrogels swollen at 37 °C in PBS show that PNiPAAm/Alg hydrogels maintain their size while PAAm/Alg hydrogels swell to almost 3 times their original size (Figure 7C). Swelling behaviors were similar in other aqueous media including cell culture media + 10% human serum or media + 10% pooled human saliva, suggesting that the swelling behavior of PNiPAAm/Alg hydrogels will be similar in

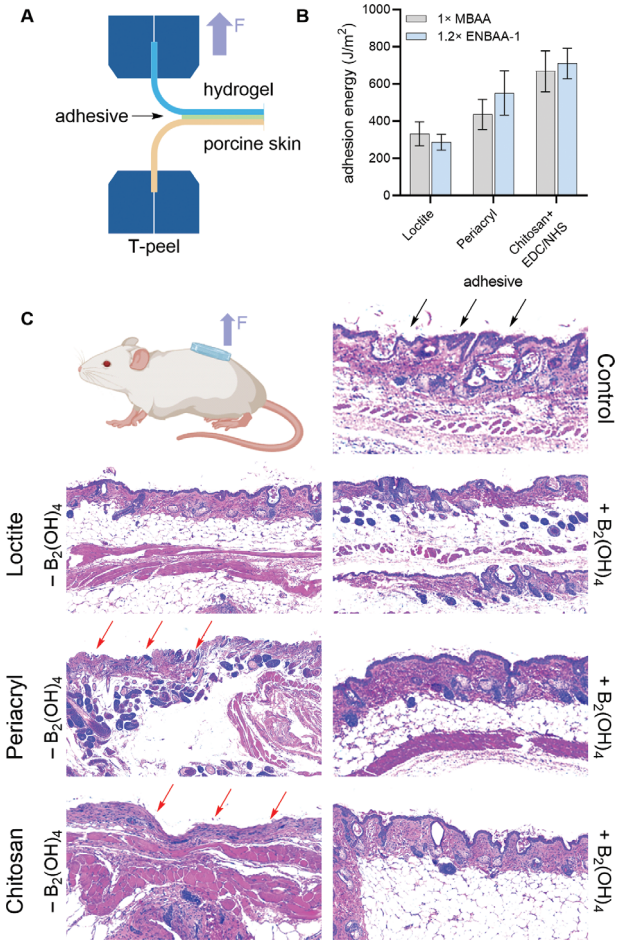

Figure 6. Analysis of the strength of adhesion of degradable hydrogels to tissues. A) Illustration of T-peel test on porcine skin. B) Adhesion energies of degradable hydrogels on porcine skin. Energies were measured using the T-peel test. Loctite, Periacryl, chitosan + EDC/sulfo-NHS were used as adhesives. Mean values are shown, and error bars represent ± SD, (n = 3). C) H&E images of mice skin after adhesion and removal of PAAm/Alg hydrogels cast with ENBAA-1 crosslinker. Aqueous $B_2(OH)_4$ (500 μM, 30 min) was used to degrade the hydrogels.

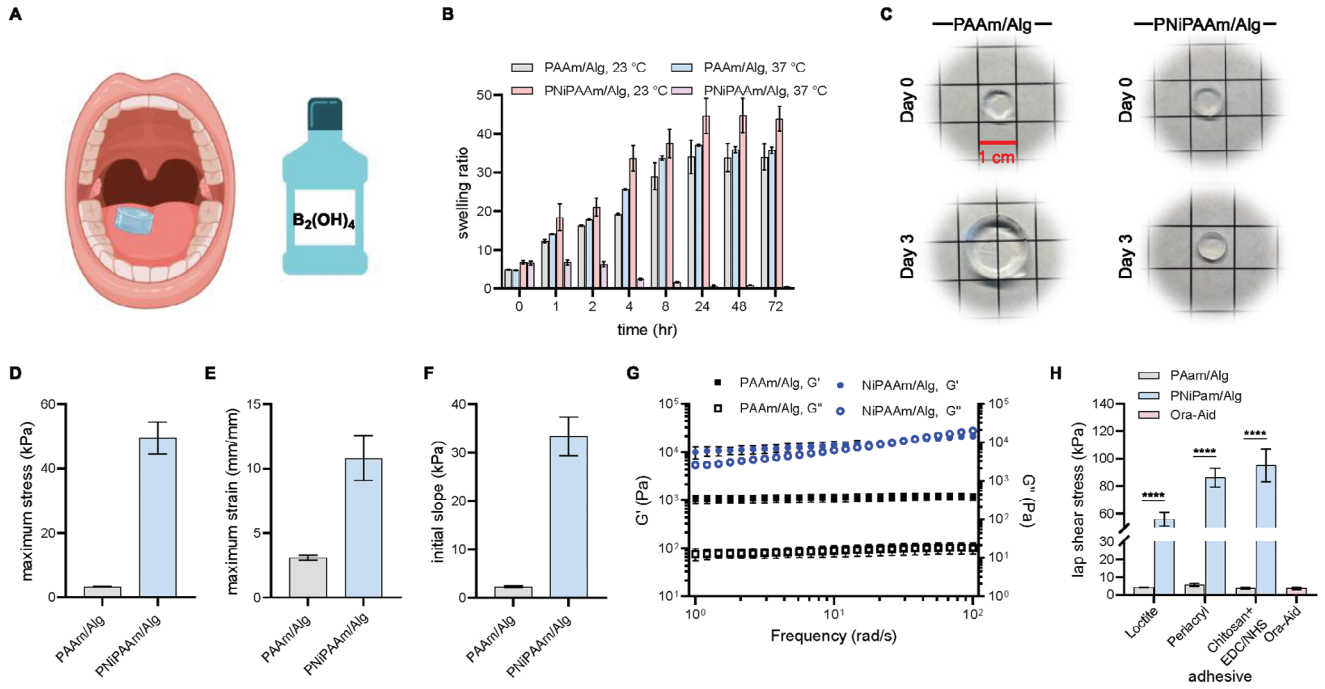

Figure 7. PNiPAAm/Alg hydrogels employed as intraoral hydrogel wound dressings. A) Illustration of the use of PNiPAAm/Alg hydrogels as anti-swelling and degradable intraoral hydrogel wound dressings together with aqueous tetrahydroxydiboron as the chemical inducer applied as a mouth wash. B) Swelling ratios of PAAm/Alg and PNiPAAm/Alg hydrogels swollen in PBS, pH 7.4 at 23 or 37 °C for 3 d. Mean values are shown, and error bars represent ± SD ($n = 3$). C) Photos of PAAm/Alg and PNiPAAm/Alg hydrogels before and after swelling in PBS, pH 7.4 at 37 °C for 3 d. D) Maximum stress, E) maximum strain, and F) initial slopes of the stress-strain curves in the strain range of 0–0.5 mm mm^{-2} of swollen PAAm/Alg and PNiPAAm/Alg hydrogels in PBS, pH 7.4 at 37 °C for 3 d. Mean values are shown, and error bars represent ± SD ($n = 3$). G) Viscoelastic responses of swollen PAAm/Alg and PNiPAAm/Alg hydrogels in PBS, pH 7.4 at 37 °C for 3 d. Mean values are shown, and error bars represent ± SD ($n = 3$). H) Lap shear stress of swollen PAAm/Alg and PNiPAAm/Alg hydrogels in PBS, pH 7.4 at 37 °C for 3 d on porcine skin pre-treated with pooled human saliva. Adhesives used include Loctite, Periacryl, chitosan + EDC/sulfo-NHS and Ora-Aid. Mean values are shown, and error bars represent ± SD ($n = 3$), as analyzed by a one-way ANOVA with post hoc *t*-tests with Bonferroni correction, ****$p < 0.0001$.

an intraoral environment (Figure S17; Figure S18, Supporting Information).

Swelling or deswelling of hydrogels influences their mechanical properties. When comparing the maximum stress, strain, initial slopes of the stress-strain curves, and viscoelastic properties of swollen hydrogels, swollen PNiPAAm/Alg hydrogels dramatically outperform swollen PAAm/Alg hydrogels. Moreover, swollen PNiPAAM/Alg hydrogels outperformed unswollen PNiPAAm/Alg hydrogels (Figure S19, Supporting Information), reaching maximum stress and strain of 48 kPa and 11 mm mm^{-1}, respectively (Figure 7D–F). Viscoelastic responses of swollen PAAm/Alg and PNiPAAm/Alg hydrogels in various media were also evaluated (Figure 7G; Figures S20,S21, Supporting Information). The storage modulus G' of PNiPAAm/Alg hydrogels was nearly 10-fold greater compared to that of PAAm/Alg hydrogels. Additionally, hydrogels that were swollen in media + human serum or media + human saliva showed comparable G′ and G″ to hydrogels swollen in PBS, pH 7.4, suggesting that the enamine *N*-oxides are stable in biological media.

Again, because adhesion energies cannot be decoupled from the toughness of the hydrogel, we hypothesized that swollen PNiPAAm/Alg hydrogel adhesives would outperform the swollen PAAm/Alg hydrogel adhesives. To evaluate the adhesive energies most applicable for intraoral applications, lap shear stress of swollen hydrogels were measured (Figure 7H). Lap shear stress of PNiPAAm/Alg hydrogels on porcine skin were an order of magnitude higher than those of PAAm/Alg hydrogels as well as those of the commercially available intraoral hydrogel adhesive Ora-Aid. The tissues were pre-incubated with pooled human saliva before adhesion for 2 min. The saliva had minimal effect on the adhesion energies of all three adhesives.

Degradation of PNiPAAm/Alg hydrogels was also evaluated in a similar manner to that of PAAm/Alg hydrogels. Because ENBAA-1 was used to fabricate the PNiPAAm/Alg hydrogels, the degradation trends were similar to those of PAAm/Alg hydrogels (**Figure** 8A). Stress-strain curves of hydrogels exposed to aqueous $B_2(OH)_4$ for 10 min showed a concentration dependent degradation profile. Again, the maximum stresses, fracture energies, and the initial slopes of the stress–strain curves of PNiPAAm/Alg hydrogels were indicative of the significant degradation of mechanical properties as the concentration of the $B_2(OH)_4$ was increased (Figure 8B–D). It was difficult to measure the fracture energies of hydrogels exposed to $B_2(OH)_4$ with concentrations greater than 100 μM because rapid degradation led to formation of an amorphous gel. It is interesting to note that hydrogels exposed to 100 μM aq. $B_2(OH)_4$ showed no loss in the initial slopes

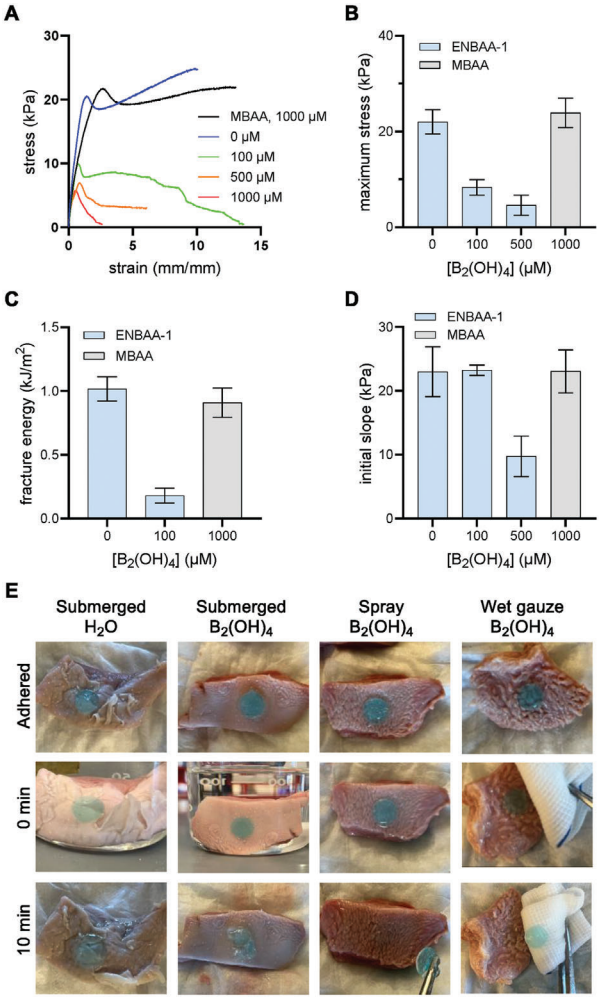

Figure 8. Degradation profiles of swollen PNiPAAm/Alg hydrogels. A) Stress–strain curves of swollen PNiPAAm/Alg hydrogels exposed to various concentrations of $B_2(OH)_4$ for 10 min 23 °C. B) Maximum stress, C) fracture energy, and D) initial slopes of the stress-strain curves in the strain range of 0–0.5 mm mm^{-2} of swollen PNiPAAm/Alg hydrogels exposed to various concentrations of $B_2(OH)_4$ for 10 min at 23 °C. Mean values are shown and error bars represent ± SD (n = 3). E) Ex vivo application of PNiPAAm/Alg hydrogels adhered to and removed from pork tongue. Hydrogels were adhered using chitosan + EDC/sulfo-NHS. Solution of $B_2(OH)_4$ (500 μM) was applied in 3 different ways for 10 min at 23 °C: 1) submerged, 2) sprayed or 3) applied by wet gauze.

of the stress-strain curves, which suggests incomplete degradation; however, the stress-strain curves show a sharp drop in the stress as the strain starts to increase after the inflection point. A certain force is required to observe loss in mechanical properties of hydrogels in tensile tests,[48,49] but this does not mean that the dissociation of the ENBAA-1 crosslinker is absent. Degradation of PNiPAAm/Alg hydrogels exposed to various concentrations of aqueous $B_2(OH)_4$ for 3 min was also explored (Figure S22, Supporting Information).

Cell viability assays were also performed with PNiPAAm/Alg hydrogels to confirm their biocompatibility. Prior to assays, the gels were incubated with PBS pH 7.4 for 3 d at 37 °C and the media was exchanged every 24 h to remove any remaining unreacted monomers to maximize biocompatibility. L929 cells were exposed to PNiPAAM/Alg hydrogels that had been pre-incubated in PBS, pH 7.4 for 3 d (Figure S23, Supporting Information). The cells were incubated with the hydrogels for 72 h, then treated with $B_2(OH)_4$ to induce hydrogel degradation. After 0.5 h, the cells were treated with Calcein AM and ethidium homodimer 1 to visualize live and dead cells. Cells that were treated with both the hydrogel and aqueous $B_2(OH)_4$ showed cell viabilities >95%. Moreover, PAAm/Alg hydrogels have been reported previously as biocompatible intraoral wound dressings.[84]

To evaluate the feasibility of removing PNiPAAm/Alg hydrogels from tissue, the diboron-mediated hydrogel degradation approach was evaluated on pork tongue in an ex vivo setting at 23 °C (Figure 8E; Figure S24–S29, Supporting Information). Hydrogel disks were first adhered to pork tongue using Loctite, Periacryl, or chitosan + EDC/sulfo-NHS. Then, aqueous solutions of $B_2(OH)_4$ (500 μM) were applied to the tissue in three different ways for 10 min: 1) the tissue was submerged in a diboron solution to simulate the delivery of the reagent as a mouth wash, 2) the diboron solution was sprayed directly onto the hydrogel with a spray bottle, completely covering the surface of the tissue, and 3) a wet gauze saturated with diboron solution was placed over the hydrogel. Photos show that when the hydrogel-tissue adduct was submerged in water without diboron treatment, the hydrogel remained adhered. Application of diboron solution by any of the three methods resulted in quick and easy removal of the hydrogel. Submerging the hydrogel in the aqueous $B_2(OH)_4$ solution proved to be most effective at degrading the hydrogel, but applying solutions of diboron via either spray bottle or wet gauze was enough to degrade the hydrogel for easy removal. Application of the aqueous solution of diboron for 5 min also resulted in efficient removal of the hydrogels (Figure S30, Supporting Information). The removability of PNiPAAm/Alg hydrogels was also evaluated at 37 °C (Figures S31–S35, Supporting Information). The photos demonstrate that diboron solutions effectively induce degradation and removal of the hydrogels at physiologically relevant temperatures within 5 min. Chemically inducible and degradable hydrogels with its fast degradation times and efficient removability coupled with the biocompatibility of the diboron reagent are effective in circumstances where repeated attachment and detachment of hydrogels is necessary, like in the oral cavity.

PNiPAAm/Alg hydrogels were designed to function as a degradable intraoral wound dressing in the presence of diboron reagents, so it was necessary to assess the safety of $B_2(OH)_4$ when swallowed. In vivo maximum tolerated dose (MTD) studies of $B_2(OH)_4$ were conducted in mice to prove the safety of the $B_2(OH)_4$ solutions (**Figure 9A**). Nude mice were administered 0 (H_2O vehicle), 25, 75, and 150 mg kg^{-1} doses of aqueous $B_2(OH)_4$ solution via oral gavage. Five consecutive daily doses were administered, and the survival rate, weight, and food consumption of the mice were recorded over 14 d (Figure 9B,C). All of the mice in the study survived and showed no signs of weight loss or restriction in their diet. The byproduct of $B_2(OH)_4$ when reacted with *N*-oxides is boric acid, which is widely used as a buffering component in pharmaceutical formulations. These MTD studies show that $B_2(OH)_4$ is safe for ingestion by mice even at 200 mM

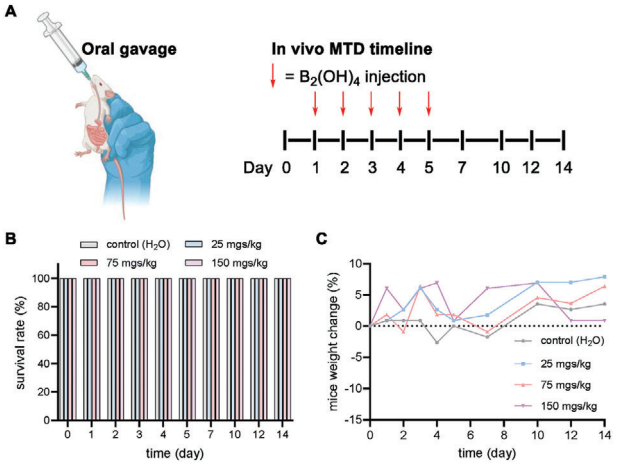

Figure 9. Maximum tolerated dose (MTD) study for administration of $B_2(OH)_4$ by oral gavage in mice. A) Illustration of oral gavage and timeline of the MTD study. B) Survival rate (%), and C) weight change (%) of mice administered with $B_2(OH)_4$ every 24 h for 5 consecutive days. Mean values are shown ($n = 5$).

concentrations and volumes up to 200 µL repeatedly over multiple days.

4. Conclusion

We have described bioorthogonally degradable tough hydrogels that can function in both dry and wet environments. Employing enamine *N*-oxide bisacrylamide as a covalent crosslinker for PAAm/Alg or PNiPAAm/Alg hydrogels enables these hydrogels to be degraded by treatment with $B_2(OH)_4$. We were able to identify the most appropriate crosslinker by evaluating crosslinkers of various lengths, and we were able to identify the optimal concentration of the crosslinker most effective for fabricating tough hydrogels with comparable mechanical properties to those of their nondegradable PAAm/Alg or PNiPAAm/Alg counterparts. The degradation is inducible, and the degradation kinetics are rapid. The factor limiting the rate of degradation is the diffusion of $B_2(OH)_4$ solution into the hydrogel for hydrogels of the dimensions and geometries evaluated in this study. High biocompatibility of both the hydrogels and $B_2(OH)_4$ suggest their potential use in wound dressings and allows for repeated attachment and detachment to the adhered tissue without causing secondary skin damage.

We were able to circumvent the swelling property of PAAm/Alg hydrogels by switching the covalently linked polymer network to PNiPAAm polymers. This allowed the PNiPAAm/Alg gels to be used in constantly wet and damp biological environments. PNiPAAm/Alg hydrogels also demonstrated inducible degradation with fast kinetics. PNiPAAm/Alg hydrogels exhibit potential for use in intraoral hydrogel wound dressings. In vivo MTD studies involving the administration of diboron solution through oral gavage demonstrates the low toxicity of tetrahydroxydiboron and its potential to be used as the chemical stimulus for the induction of degradation of hydrogels fabricated with ENBAA-1 as the covalent crosslinker.

The promising properties of these hydrogels are accompanied by limitations inherent to chemically degradable systems. Chemical reagent-responsive materials require an exogenous stimulus, and the difficulties in achieving precise spatial control of the exogenous stimulus makes certain applications unfeasible. For example, the need for a chemical stimulus makes the degradation of hydrogels implanted in poorly accessible locations challenging. Moreover, the lack of precision in spatial control over the site of degradation is inevitable for small molecule-responsive materials where the reagent can diffuse away from the site of application. However, certain applications can benefit from the lack of spatial constraint, especially in scenarios where materials have large dimensions, are amorphous, or have irregular geometries. The ability of the chemical stimulus to spread out and cover a larger area can be beneficial and is a unique feature of our method, which is difficult to replicate using other types of stimuli. Chemically degradable hydrogels thus offer compensatory benefits that could offset these limitations.

Despite these limitations, the inducibly degradable hydrogels described in this study provide a novel alternative to existing degradable materials. This degradable system exhibits rapid degradation kinetics, excellent biocompatibility, minimal invasiveness, and greater accessibility, broadening the potential use of degradable materials in biomedical applications. Importantly, bioorthogonally degradable materials function in an orthogonal space compared to biodegradable materials and existing inducibly degradable systems such as photodegradable materials. Looking ahead, enamine *N*-oxide-based hydrogels have potential applications that extend beyond the demonstrations described in this study, offering potential use in areas such as thermal stabilization of biologics[85] and as drug-loaded, tissue-protective, and degradable hydrogels in tissue ablation therapies.[86] In addition, we expect that incorporation of the enamine *N*-oxide motif into polymers by means other than as the crosslinking agent will provide alternative and powerful ways to place the functional properties of a material under small molecule control.

5. Experimental Section

*Synthesis of Bis-Boc-Bromoenamine N-Oxide (**9**)*: 2,2,2-Trifluoroethanol (TFE) in chloroform (20% v/v, 20 mL) was added to a 25 mL round bottom flask charged with hydroxylamine 1 (3.47 g, 18.2 mmol, 2.00 equiv) and bromoalkyne 8 (2.94 g, 9.14 mmol, 1 equiv). The vial was flushed with nitrogen, sealed with a septum cap and Parafilm, then heated to 50 °C in an oil bath. After 3 h, the reaction was cooled to room temperature and concentrated under reduced pressure. The crude oil was purified by flash column chromatography on silica gel (eluent: 10→40% CMA in chloroform) to provide bis-Boc-bromoenamine *N*-oxide 9 (4.30 g, 92%) as a white foam.

^{1}H NMR (500 MHz, CD_3OD) δ 7.48 (t, J = 5.6 Hz, 1H), 4.72 (qd, J = 14.5, 5.7 Hz, 2H), 4.07–3.90 (m, 1H), 3.52–3.35 (m, 6H), 3.17 (d, J = 4.9 Hz, 2H), 3.14 (d, J = 4.8 Hz, 2H), 1.43 (s, 9H), 1.43 (s, 9H).

^{13}C NMR (126 MHz, CD_3OD) δ 158.7, 158.5, 158.3, 131.5, 128.7, 80.5, 80.3, 69.0, 63.9, 60.9, 42.1, 41.3, 36.2, 28.9, 28.9.

FTIR (thin film) cm^{-1}: 3332 (br), 2984 (w), 1692 (s), 1524 (m), 1454 (w), 1252 (m), 1170 (s), 1030 (w).

HRMS (ESI) (*m/z*): calc'd for $C_{19}H_{35}BrN_4O_7$ $[M+H]^+$: 511.1762, found: 511.1786.

TLC (30% CMA in chloroform), *Rf*: 0.14 ($KMnO_4$).

*Synthesis of Bis-Boc-Enamine N-Oxide (**3**)*: A round bottom flask was charged with bis-Boc-bromoenamine *N*-oxide **9** (3.27 g, 6.36 mmol, 1 equiv) and purged with nitrogen. Tetrahydrofuran (200 mL) was then added via syringe, the reaction mixture was cooled to– 78 °C using an acetone-dry ice bath, and *n*-butyllithium (1.9 M in hexanes, 3.68 mL, 7.00 mmol, 1.10 equiv) was added dropwise via syringe. After 20 min, the reaction was quenched with deionized water (1 mL) and warmed to room temperature by removing the acetone-dry ice bath. The resulting crude mixture was concentrated under reduced pressure and purified by flash column chromatography on silica gel (eluent: 30→60% CMA in chloroform) to provide bis-Boc-enamine *N*-oxide **3** (2.09 g, 76%) as a white foam.

^{1}H NMR (500 MHz, CD_3OD) δ 6.56 (dt, J = 13.3, 5.0 Hz, 1H), 6.49 (d, J = 13.4 Hz, 1H), 4.68 (d, J = 4.9 Hz, 2H), 3.61–3.38 (m, 4H), 3.25 (s, 3H), 3.22–2.97 (m, 4H), 1.43 (s, 9H), 1.43 (s, 9H).

^{13}C NMR (126 MHz, CD_3OD) δ 157.2, 156.9, 156.7, 140.7, 123.0, 79.1, 78.7, 68.9, 60.6, 58.1, 40.5, 39.8, 34.9, 27.4, 27.3.

FTIR (thin film) cm^{-1}: 3343 (br), 2974 (w), 1700 (s), 1524 (m), 1415 (m), 1364 (m), 1252 (m), 1167 (s), 1039 (w), 779 (w)

HRMS (ESI) (*m/z*): calc'd for $C_{19}H_{36}N_4O_7$ $[M+H]^+$: 433.2657, found: 433.2655.

TLC (60% CMA in chloroform), R*f*: 0.29 ($KMnO_4$).

Synthesis of Enamine N-Oxide Bisacrylamide (ENBAA-1): Trifluoroacetic acid in dichloromethane (20% v/v, 3 mL) was added to a round bottom flask charged with bis-Boc-enamine *N*-oxide **3** (521 mg, 1.21 mmol, 1 equiv) at room temperature. After 3 h, the reaction mixture was concentrated under reduced pressure. To the crude oil was added deionized water (8 mL) followed by sodium bicarbonate (709 mg, 8.44 mmol, 7.00 equiv) portion-wise at room temperature. The flask was covered in foil, and *N*-acryloxysuccinimide (428 mg, 2.53 mmol, 2.10 equiv) was added to the solution. After 1 h, the reaction mixture was purified by automated C_{18} reverse phase column chromatography (30 g C_{18} silica gel, 25 µm spherical particles, eluent: H_2O + 0.2% Et_3N (2 CV), gradient 0→100% MeCN/H_2O + 0.2% Et_3N (10 CV) to provide enamine *N*-oxide bisacrylamide ENBAA-1 (329 mg, 80%, 2 steps) as a white solid.

^{1}H NMR (500 MHz, CD_3OD) δ 6.60 (dt, J = 13.0, 5.0 Hz, 1H), 6.56–6.51 (m, 1H), 6.29–6.17 (m, 4H), 5.76–5.63 (m, 2H), 4.70 (dd, J = 5.1, 1.6 Hz, 2H), 3.76–3.57 (m, 3H), 3.57–3.49 (m, 1H), 3.38 (td, J = 6.1, 3.6 Hz, 2H), 3.30–3.24 (m, 5H).

^{13}C NMR (126 MHz, CD_3OD) δ 167.0, 166.8, 157.0, 140.6, 130.7, 130.4, 125.7, 125.4, 123.3, 68.6, 60.7, 58.4, 40.1, 38.9, 33.9.

FTIR (thin film) cm^{-1}: 3340 (br), 2974 (w) 1696 (s), 1528 (m), 1453 (m), 1364 (m), 1252 (m), 1170 (m), 998 (w), 779 (w).

HRMS (ESI) (*m/z*): calc'd for $C_{15}H_{24}N_4O_5$ $[M+H]^+$: 341.1819, found: 341.1823.

Preparation of PAAm/Alg Hydrogels: 2.2% Sodium alginate solution was prepared by dissolving high-molecular-weight sodium alginate (110 mg, MVG, NovaMatrix) and low-molecular-weight sodium alginate (110 mg, VLVG, NovaMatrix) in Hank's Balanced Salt Solution (HBSS, 10 mL, pH 7.4). Acrylamide (1.35 g), *N,N,N′,N′*-tetramethylethylenediamine (TEMED, 8 µL), and methylene bisacrylamide (MBAA, 123 mM in water, 36 µL) or enamine *N*-oxide bisacrylamide (ENBAA-1, 156 mM in water, 36 µL) covalent crosslinker was added to the fully dissolved sodium alginate solution and drawn into a syringe. A second syringe containing ammonium persulfate (APS, 226 µL of 6.6% w/v in water) and calcium sulfate dihydrate ($CaSO_4 \cdot 2H_2O$, 0.75 M in water, 191 µL) was connected to the syringe containing the alginates, acrylamide, TEMED, and covalent crosslinker with a female-female luer connector and syringe mixed. For ENBAA-2 and ENBAA-3, refer to Table S1 (Supporting Information). The gel was cast into glass molds (75 mm × 80 mm × 1.5 mm, w × l × d), placed in a sealed plastic bag away from light, and left to crosslink for 24 h. After 24 h, the gel was removed from the mold, placed in a sealed plastic bag, and stored at 4 °C.

Hydrogel Mechanical Properties: Tensile tests were performed in tension (Instron 3400-SC1, 100 N load cell) and stress-strain curves were obtained to evaluate the maximum stretch, stress, and the initial slopes of the stress–strain curves of the hydrogels. The hydrogel was glued between two glass plates at each end, resulting in rectangular specimens measuring 70 mm × 5 mm × 1.5 mm (w×l×d). All tensile tests were performed in air at room temperature using a tensile testing machine with a 100 N load cell. The rate of tension was fixed at 50 mm min^{-1} and the hydrogel was pulled until rupture. From the stress-strain curve, the maximum stretch, maximum strain, and the initial slopes of the stress-strain curves were calculated. The initial slopes of the stress-strain curves were obtained by linear fitting. For PAAm/Alg hydrogels, the strain range was set to 0–1 mm mm^{-2}. For PNiPAAm/Alg hydrogels, the strain range was set to 0–0.5 mm mm^{-2}. The fracture energy of a gel was assessed following the method outlined by Rivlin and Thomas.[66] Two samples of identical gel, one unnotched and one notched, were evaluated. Rectangular hydrogel specimens with dimensions: width (w) = 70 mm, thickness (t) = 1.5 mm, and length (l) = 5 mm underwent the tensile testing protocol outlined above. The unnotched gel was placed under tension until rupture, and the resultant force-length curve was analyzed to determine the work done (U(L)). For the notched sample, a 40 mm-long notch was created using a razor blade, and the critical clamp distance (L_c) at which the notch transitions into a running crack was measured. The fracture energy was then calculated using Equation 1:

$$\text{Fracture energy } \left(\text{kJ/m}^2\right) = U\left(L_c\right) / (w)\,(t) \quad (1)$$

Viscoelastic Responses of PAAm/Alg Hydrogels determined by DMA: The viscoelastic responses of PAAm/Alg hydrogels were determined using a Mettler Toledo DMA 1 instrument. Compression frequency sweep tests at 0.1% strain were carried out over the frequency range of 0.1–30 Hz. PAAm/Alg gels were cast following the general procedure. Hydrogels were punched into disks (8.0 mm diameter, 1.5 mm thickness) for each measurement. The storage modulus E′ and loss modulus E″ were recorded.

Degradation of PAAm/Alg Hydrogels with aq. $B_2(OH)_4$: PAAm/Alg hydrogels were cast following the general procedures. Tensile tests were performed following the general procedures to determine the maximum stress and the initial slopes of the stress-strain curves. Fracture energy was determined following the general procedures. Prior to tensile test, only the sample region undergoing stress was submerged in aq. $[B_2(OH)_4]$ for the specified time.

Discrete Viscoelastic Responses of PAAm/Alg Hydrogels Exposed to aq. $B_2(OH)_4$: PAAm/Alg hydrogels were cast following the general procedures. Rheology tests were performed on TA Instruments Discovery HR 2 to evaluate the trends of hydrogels exposed to aqueous $[B_2(OH)_4]$ ranging from 10 mM to 100 µM. A rubber spacer (5 mm diameter, 5 mm thick) was attached to the bottom plate. A 150Cw sandpaper was fixed on the bottom plate and 800Cw sandpaper was fixed to the top spindle to provide sufficient grip on the samples during measurement. Viscoelastic responses of nondegradable and degradable hydrogels aqueous $B_2(OH)_4$ were measured, and the shear moduli were recorded. Hydrogels disks (1.0 mm or 1.5 mm thick, 5 mm diameter) were prepared for evaluation. Six $[B_2(OH)_4]$ were chosen: 10 mM, 3 mM, 1 mM, 500 µM, 100 µM, and 0 µM. Initial oscillation tests were performed to obtain initial storage and loss moduli. The top spindle was raised to 5 mm height, and aqueous $B_2(OH)_4$ (5 mL) solution was added to the bottom plate. Subsequently, when the spindle reached the geometry gap, the gel's moduli were recorded. The geometry gap was set at 800 µm for the 1.0 mm thick samples and 1200 µm for the 1.5 mm thick samples. After each measurement, the top spindle was sufficiently raised to increase the contact surface area of aqueous $B_2(OH)_4$ to the gel disks. It was essential to allow the diboron solution to diffuse into the gel from the bottom and the side surface of the hydrogel disk. This procedure was repeated for 36 cycles. The holding time was 10 s for the first 6 cycles and 1 minute for the remaining. For each cycle, the oscillation test was performed at 20 °C with 1 Hz frequency and 5% shear strain amplitude.

Cell Viability Assay: For cell culture, L929 fibroblasts were cultured in modified MEM 1× with l-glutamine containing 10% horse serum (Fisher), 100 units mL^{-1} penicillin and 0.1 mg mL^{-1} streptomycin (Sigma) in a humidified chamber at 37 °C under an ambient atmosphere with 5% CO_2 unless otherwise stated. All cell lines were acquired from ATCC. Cells were passaged and dissociated with 0.25% trypsin, 0.1% EDTA in HBSS (Corning). All cells tested negative for mycobacteria with the MycoAlert

PLUS Mycoplasma Detection Kit (Lonza) following manufacturer's protocol. To prepare 96-well plate, an aqueous solution of human fibronectin (10 μg mL^{-1}, 100 μL, Corning) was added to each well. The plate was gently shaken to distribute the solution evenly, incubated at room temperature for 0.5 h, washed using autoclaved deionized water (100 μL) then autoclaved PBS, pH 7.4 (100 μL), and air-dried for 0.5 h at room temperature.

L929 fibroblasts were seeded in an opaque 96-well plate at a density of 10000 cells per well in media (100 μL, MEM containing 10% horse serum, 100 units mL^{-1} penicillin, 0.1 mg mL^{-1} streptomycin). PBS (pH 7.4, 100 μL) was added to the edge wells. The cells were incubated in a humidified chamber at 37 °C with 5% CO_2. After 24 h, the media was aspirated and replaced with media (100 μL, MEM supplemented with 10% FBS, 100 units mL^{-1} penicillin, 0.1 mg mL^{-1} streptomycin) containing tetrahydroxydiboron. Treatment concentrations started at 50 mM and was serially diluted 2.5-fold across nine wells. Vehicle controls corresponding to the treatment consisted of complete growth media (100 μL). The treated plates were incubated at 37 °C with 5% CO_2 for 0.5 or 3 h after which the media was removed, the cells were washed twice with PBS pH 7.4, and the solution was replaced with complete growth media (100 μL). After incubating at 37 °C with 5% CO_2 for 24 h, the plates were removed from the incubator and allowed to equilibrate at room temperature for 10 min. CellTiter-Glo 2.0 reagent (50 μL, Promega) was added directly to each well and mixed gently. The plates were incubated at room temperature for 10 min to stabilize the luminescence signal and then analyzed by a microplate reader (Clariostar Plus, BMG Labtech).

LIVE/DEAD Cell Viability Assay: For the preparation of a 24-well plate, an aqueous solution of human fibronectin (10 μg mL^{-1}, 500 μL, Corning) was added to each well. The plate was gently shaken to distribute the solution evenly, incubated at room temperature for 0.5 h, washed using autoclaved deionized water (500 μL) then autoclaved PBS, pH 7.4 (500 μL), and air-dried for 0.5 h at room temperature. L929 fibroblasts were seeded in a 24-well plate at a density of 5000 cells per well in media (500 μL, MEM containing 10% horse serum, 100 units mL^{-1} penicillin, 0.1 mg mL^{-1} streptomycin). The cells were incubated in a humidified chamber at 37 °C with 5% CO_2. After 24 h, the media was aspirated and replaced with media (100 μL, MEM supplemented with 10% FBS, 100 units mL^{-1} penicillin, 0.1 mg mL^{-1} streptomycin) and hydrogel disks were introduced to each well. Vehicle controls corresponding to the treatment consisted of complete growth media (500 μL). The treated plates were incubated at 37 °C with 5% CO_2. After 72 h, the media was aspirated and replaced with media (1 mL, MEM supplemented with 10% FBS, 100 units mL^{-1} penicillin, 0.1 mg mL^{-1} streptomycin, 500 μM tetrahydroxydiboron), and incubated at 37 °C with 5% CO_2. After 0.5 h, the plates were removed from the incubator and allowed to equilibrate at room temperature for 10 min. The media was aspirated and replaced with an aqueous solution of Calcein AM and ethidium homodimer-1 (EthD-1) (500 μL, 2 μM Calcein AM, 4 μM EthD-1, Invitrogen) then mixed gently. The plates were incubated at room temperature for 20 min and then imaged by fluorescence microscopy.

Fluorescence Microscopy and Cell Counting: Wells were imaged at the Confocal and Light Microscopy Core at Dana-Farber Cancer Institute using a Zeiss 980 confocal microscope. Images were acquired with a 10× objective at 0.16 micron $pixel^{-1}$ using a Hamamatsu camera. Cells stained with Calcein AM were imaged with a 482/35 filter (excitation) and a 536/75 filter (emission) and false-colored green and cells stained with Ethd-1 were imaged with a 560/40 filter (excitation) and a 630/75 filter (emission) and false-colored red. Five images per well, ($n = 3$) were analyzed using CellProfiler software with a custom pipeline. Cells stained with Calcein AM, C_A and cells stained with Ethd-1, C_D were counted. Cell viability was calculated from Equation 2:

$$\text{Cell viability } (\%) = C_A / (C_A + C_D) \times 100 \quad (2)$$

Adhesive Application and Adhesion Energy Measurement: Loctite (4541, Henkel, gel-type cyanoacrylate), Periacryl (high viscosity cyanoacrylate), and chitosan (2% w/v in 0.5 M MES buffer, pH 4.5) with 1-ethyl-3-(3-dimethylaminopropyl)carbodiimide (EDC, 12 mg mL^{-1}) and *N*-hydroxysulfosuccinimide sodium salt (sulfo-NHS, 12 mg mL^{-1}) were used as adhesives. For Loctite and Periacryl, 21 mg cm^{-1} was applied to the surface of the tissue, and PAAm/Alg hydrogel was applied and compressed for 20 min. For chitosan with EDC and sulfo-NHS, 25 μL cm^{-2} was applied to the surface of the tissue, and PAAm/Alg hydrogel was applied and compressed for 20 min.

Adhesion energy was measured by T-peel test using an Instron 3400 tensile testing instrument with a 100 N load cell under a uniaxial tension with a rate of 50 mm min^{-1} in air at room temperature. A strip of hydrogel (70 × 15 × 1.5 mm^3) was adhered to pork skin with one end open, forming a bilayer with an edge crack. The back of the hydrogel was glued to a rigid polyethylene terephthalate film (3M) with Krazy Glue to ensure that all work done by the machine would be equal to the energy dissipated at the crack tip. The free ends were attached in between two glass plates to which the machine grips were attached. Force-displacement curves were obtained, and adhesion energy was calculated using Equation 3:

$$\text{Adhesion energy } \left(J\,m^{-2}\right) = 2 \times (\text{plateau value of F}) / \text{width} \quad (3)$$

Ex Vivo Evaluation of Application and Removal of PAAm/Alg Hydrogel: Ex vivo application and removal of PAAm/Alg hydrogels were evaluated on the skin of euthanized mice. Nude mice were donated by Dana-Farber Cancer Institute, Animal Resources Facility. Mice were euthanized with CO_2 followed by cervical dislocation. Mice were skinned and the skin was used without any further treatment. Loctite (4541, Henkel, gel-type cyanoacrylate-based adhesive), Periacryl (high viscosity cyanoacrylate-based adhesive) and chitosan (2% w/v in 0.5 M MES pH 4.5) with 1-ethyl-3-(3-dimethylaminopropyl)carbodiimide (EDC, 12 mg mL^{-1}) and *N*-hydroxysulfosuccinimide sodium salt (sulfo-NHS, 12 mg mL^{-1}) were used as adhesives. A strip of hydrogel (40 × 10 × 1.5 mm^3) was adhered to the surface of mice skin. For Loctite and Periacryl, 21 mg cm^{-1} was applied to the surface of the tissue. Then PAAm/Alg hydrogel was applied and compressed for 20 min. For chitosan with EDC and sulfo-NHS, 25 μL cm^{-2} was applied to the surface of the tissue. Then PAAm/Alg hydrogel was applied and compressed for 20 min.

Hydrogels were either removed with or without degradation. For removal of hydrogels without degradation, the back of the hydrogel was glued to a rigid polyethylene terephthalate film (3M) with KrazyGlue to ensure that all work done when removing the hydrogel would be equal to the energy dissipated at the crack tip. For removal of hydrogels after degradation, the tissue with adhered hydrogel was submerged in an aqueous solution of $B_2(OH)_4$ (500 μM in H_2O, 20 mL) for 30 min in air at room temperature. The tissue was then removed from the $B_2(OH)_4$ solution, and the degraded hydrogel was wiped away with a tissue (KimTech). The tissues were collected and submerged in 10% formalin in PBS, pH 7.4 (5 mL) at 4 °C for 24 h. Tissues were then washed with PBS, pH 7.4 (2 × 10 mL), then stored in 70% ethanol (5 mL) at 4 °C for hematoxylin and eosin (H&E) staining.

Tissue samples were embedded in paraffin, sectioned, mounted, and stained with hematoxylin and eosin (H&E) by the Rodent Histopathology Core at Harvard Medical School. H&E slides were imaged at the Confocal and Light Microscopy Core at Dana-Farber Cancer Institute using a Nikon Ti Eclipse. Images were acquired with a 10× objective at 5.68 micron $pixel^{-1}$ using a DMC6200 camera from Leica.

Preparation of PNiPAAm/Alg Hydrogels: 2.2% Sodium alginate solution was prepared by dissolving high-molecular-weight sodium alginate (110 mg, MVG, NovaMatrix) and low-molecular-weight sodium alginate (110 mg, VLVG, NovaMatrix) in HBSS (10 mL, pH 7.4). To a fully dissolved sodium alginate solution was added *N*-isopropyl acrylamide (1.35 g), *N,N,N′,N′*-tetramethylethylenediamine (TEMED, 8 μL) and methylene bisacrylamide (MBAA, 123 mM in water, 36 μL) or enamine *N*-oxide bisacrylamide (ENBAA-1, 156 mM in water, 36 μL) covalent crosslinker and drawn into a syringe. A second syringe containing ammonium persulfate (APS, 226 μL of 6.6% w/v in water) and calcium sulfate dihydrate ($CaSO_4 \cdot 2H_2O$, 0.75 M in water, 191 μL) was connected to the syringe containing the alginates, acrylamide, TEMED and covalent crosslinker with a female-female luer connector and syringe mixed. The gel was cast into glass molds (75 × 1.5 × 80 mm^3), placed in a sealed plastic bag away from light, and left to crosslink for 24 h. After 24 h, the

gel was removed from the mold and placed in a container filled with PBS pH 7.4. The gel was stored in PBS, pH 7.4 at 37 °C for 72 h prior to use.

Swelling Ratios of Degradable Hydrogels: The swelling ratios of the degradable tough hydrogels were evaluated. Cylindrical specimens (8 mm diameter, 1.5 mm height) were immersed in PBS pH 7.4 (10 mL) and incubated at 23 or 37 °C. The mass of swollen hydrogels was weighed over the course of 72 h. The swelling ratio was calculated using Equation 4:

$$Q\,(\%) = (w_2 - w_1)\,/w_1 \times 100 \quad (4)$$

where Q (%) is swelling ratio, w_2 is the weight of the hydrogel after swelling, and w_1 is the weight of the hydrogel before swelling.

Single Lap Shear Stress Measurement: Lap shear tests were conducted to evaluate the adhesion strength between the hydrogels and experimental biological surfaces. The lap shear stresses examine the resistance of hydrogels to shear forces when adhered to biological tissues. Loctite (4541, Henkel, gel-type cyanoacrylate), Periacryl (high viscosity cyanoacrylate), and chitosan (2% w/v in 0.5 M MES buffer, pH 4.5) with 1-ethyl-3-(3-dimethylaminopropyl)carbodiimide (EDC, 12 mg mL^{-1}) and *N*-hydroxysulfosuccinimide sodium salt (sulfo-NHS, 12 mg mL^{-1}) were used as adhesives. For Loctite and Periacryl, 20 mg cm^{-2} was applied to the surface of either swollen PAAm/Alg or PNiPAAm/Alg hydrogels in PBS, pH 7.4 at 37 °C over 3 d and was applied to the porcine skin and compressed for 20 min. For chitosan with EDC and sulfo-NHS, 25 µL cm^{-2} was applied to the surface of either swollen PAAm/Alg hydrogel or PNiPAAm/Alg hydrogels in PBS pH 7.4 at 37 °C over 3 d and was applied to the porcine skin and compressed for 20 min. Prior to hydrogel application, the tissues were treated with pooled human saliva (200 µL). For Ora-Aid, no adhesives were applied.

Lap shear tests were conducted with an Instron 3400 tensile testing instrument with a 100 N load cell under a uniaxial tension with a rate of 50 mm min^{-1} in air at room temperature. A strip of hydrogel (70 mm × 15 mm × 1.5 mm, l × w × h) was adhered to porcine skin, creating an overlap between the hydrogel and the tissue with an area of 50 mm × 1.5 mm. The back of the hydrogel was glued to a rigid polyethylene terephthalate film (3M) with Krazy Glue to ensure that all work done by the machine would be equal to the energy dissipated at the crack tip. The free ends were attached in between two glass plates to which the machine grips were attached. Force-displacement curves were obtained, and lap shear stresses were calculated using Equation 5:

$$\text{Lap shear stress (kPa)} = \text{maximum force/bond area} \quad (5)$$

Ex Vivo Evaluation of Adhesion and Removal of PNiPAAm/Alg Hydrogel: To evaluate the degradable and removable PNiPAAm/Alg hydrogels in an ex vivo context, PNiPAAm/Alg hydrogels were adhered to pork tongue and an aqueous solution of $B_2(OH)_4$ was applied. PNiPAAm/Alg were cast following the general procedures for hydrogel preparation and swollen in PBS pH 7.4 at 37 °C for 3 d. Blue food coloring was added during hydrogel preparation for visualization. Hydrogels were punched into disks (10 mm diameter, 1.0 mm thickness). Three adhesives were employed: 1) Loctite, 2) Periacryl and 3) chitosan + EDC and sulfo-NHS. For Loctite and Periacryl, 20 mg cm^{-2} was applied to the surface of the hydrogel. For chitosan with EDC and sulfo-NHS, 25 µL cm^{-1} was applied to the surface of the hydrogels. Pooled human saliva (70 µL) was applied to the pork tongue followed by the hydrogel. The hydrogel was compressed for 20 min. Hydrogel-tissue adducts were then treated at 23 °C with a 500 µM solution of $B_2(OH)_4$ in water in three different ways for 5 or 10 min: 1) submerging the hydrogel/tissue in a solution of $B_2(OH)_4$ to mimic swishing, 2) spraying $B_2(OH)_4$ solution using a spray bottle, or 3) applying a gauze saturated with $B_2(OH)_4$ solution. For experiments performed at 37 °C, both the tissue-hydrogel adduct and aqueous solution of diboron were pre-warmed to and maintained at 37 °C in an incubator before and during application.

In Vivo Maximum Tolerable Dose (MTD) Study of $B_2(OH)_4$: All animal experiments were performed according to procedures and protocols approved by the Dana-Farber Cancer Institute Institutional Animal Care and Use Committee (Protocol #20-019). 8-week old, female, homozygous NU/J mice (Jackson Laboratory, IMSR_JAX:002019) were dosed with aqueous solution of $B_2(OH)_4$ via oral gavage using a reusable stainless feeding needle, 20G-1.5″ curved. All $B_2(OH)_4$ solutions were prepared with autoclaved deionized water and were syringe filtered (UltraCruz, PVDF 0.22 µm, 13 mm diameter) before oral gavage. Four groups were dosed with different $B_2(OH)_4$ concentrations: 1) vehicle (0 mgs kg^{-1}, 0 mM), 2) low (25 mgs kg^{-1}, 34.3 mM), 3) medium (75 mgs kg^{-1}, 96.2 mM), and 4) high (150 mgs kg^{-1}, 205.8 mM). The highest dosage is nearing the solubility limit of $B_2(OH)_4$ in water. $B_2(OH)_4$ was dosed via oral gavage every 24 h for 5 consecutive days. Mice survival, body weight, and food intake were recorded every day for the first 5 d, then every 2–3 d for 9 d. Mice were euthanized at day 14 with CO_2 followed by cervical dislocation.

Statistical Analysis: Graphs were generated using GraphPad Prism, and all data were presented as a mean with error bars representing standard deviations. An unpaired *t*-test was used to analyze differences between two groups with Welch's post-hoc analysis. A one-way analysis of variance (ANOVA) with post hoc *t*-tests with Bonferroni correction was performed to assess differences between more than two groups. Data were deemed significant if $p < 0.05$.

Supporting Information

Supporting Information is available from the Wiley Online Library or from the author.

Acknowledgements

T.K. and J.K. conceived the project, designed the experiments, analyzed the data, and prepared the manuscript; T.K. carried out the experiments; D.M., D.H., and Y.H. carried out and analyzed data from the rheology experiments. All authors discussed the results and commented on the manuscript. This research was supported by the NSF CAREER award (2503344 and 2238040) to J.K.

Conflict of Interest

The authors declare no conflict of interest.

Data Availability Statement

The data that support the findings of this study are available in the supplementary material of this article.

Keywords

bioorthogonal, degradable, double network hydrogels, enamine *N*-oxides, intraoral wound dressings, tough hydrogels

Received: September 27, 2024
Revised: January 20, 2025
Published online: February 28, 2025

[1] X. Li, J. P. Gong, *Nat. Rev. Mater.* **2024**, *9*, 380.
[2] X. Li, Q. Sun, Q. Li, N. Kawazoe, G. Chen, *Front. Chem.* **2018**, *6*, 499.
[3] H. Cao, L. Duan, Y. Zhang, J. Cao, K. Zhang, *Signal Transduct. Target. Ther.* **2021**, *6*, 426.
[4] E. Caló, V. V. Khutoryanskiy, *Eur. Polym. J.* **2015**, *65*, 252.
[5] R. D. Kasai, D. Radhika, S. Archana, H. Shanavaz, R. Koutavarapu, D.-Y. Lee, J. Shim, *Int. J. Polym. Mater. Polym. Biomater.* **2023**, *72*, 1059.

[6] N. Joshi, J. Yan, S. Levy, S. Bhagchandani, K. V. Slaughter, N. E. Sherman, J. Amirault, Y. Wang, L. Riegel, X. He, T. S. Rui, M. Valic, P. K. Vemula, O. R. Miranda, O. Levy, E. M. Gravallese, A. O. Aliprantis, J. Ermann, J. M. Karp, *Nat. Commun.* **2018**, *9*, 1275.
[7] R. Zhong, S. Talebian, B. B. Mendes, G. Wallace, R. Langer, J. Conde, J. Shi, *Nat. Mater.* **2023**, *22*, 818.
[8] J. Li, D. J. Mooney, *Nat. Rev. Mater.* **2016**, *1*, 16071.
[9] K. Y. Lee, D. J. Mooney, *Chem. Rev.* **2001**, *101*, 1869.
[10] F. Xu, C. Dawson, M. Lamb, E. Mueller, E. Stefanek, M. Akbari, T. Hoare, *Front. Bioeng. Biotechnol.* **2022**, *10*, 849831.
[11] O. Chaudhuri, L. Gu, D. Klumpers, M. Darnell, S. A. Bencherif, J. C. Weaver, N. Huebsch, H. Lee, E. Lippens, G. N. Duda, D. J. Mooney, *Nat. Mater.* **2016**, *15*, 326.
[12] X. Lin, X. Zhao, C. Xu, L. Wang, Y. Xia, *J. Polym. Sci.* **2022**, *60*, 2525.
[13] J. P. Gong, Y. Katsuyama, T. Kurokawa, Y. Osada, *Adv. Mater.* **2003**, *15*, 1155.
[14] J.-Y. Sun, X. Zhao, W. R. K. Illeperuma, O. Chaudhuri, K. H. Oh, D. J. Mooney, J. J. Vlassak, Z. Suo, *Nature* **2012**, *489*, 133.
[15] Z. J. Wang, J. Jiang, Q. Mu, S. Maeda, T. Nakajima, J. P. Gong, *J. Am. Chem. Soc.* **2022**, *144*, 3154.
[16] S. Merino, C. Martín, K. Kostarelos, M. Prato, E. Vázquez, *ACS Nano* **2015**, *9*, 4686.
[17] A. K. Gaharwar, S. A. Dammu, J. M. Canter, C.-J. Wu, G. Schmidt, *Biomacromolecules* **2011**, *12*, 1641.
[18] Y. Okumura, K. Ito, *Adv. Mater.* **2001**, *13*, 485.
[19] Q. Chen, H. Chen, L. Zhu, J. Zheng, *J. Mater. Chem. B* **2015**, *3*, 3654.
[20] J. Li, A. D. Celiz, J. Yang, Q. Yang, I. Wamala, W. Whyte, B. R. Seo, N. V. Vasilyev, J. J. Vlassak, Z. Suo, D. J. Mooney, *Science* **2017**, *357*, 378.
[21] X. Li, S. Sheng, G. Li, Y. Hu, F. Zhou, Z. Geng, J. Su, *Adv. Healthcare Mater.* **2024**, 2400431.
[22] L. Lei, R. Cong, Y. Ni, X. Cui, X. Wang, H. Ren, Z. Wang, M. Liu, J. Tu, L. Jiang, *Adv. Healthcare Mater.* **2024**, *13*, 2302551.
[23] M. Baumgartner, F. Hartmann, M. Drack, D. Preninger, D. Wirthl, R. Gerstmayr, L. Lehner, G. Mao, R. Pruckner, S. Demchyshyn, L. Reiter, M. Strobel, T. Stockinger, D. Schiller, S. Kimeswenger, F. Greibich, G. Buchberger, E. Bradt, S. Hild, S. Bauer, M. Kaltenbrunner, *Nat. Mater.* **2020**, *19*, 1102.
[24] M. Cianchetti, C. Laschi, A. Menciassi, P. Dario, *Nat. Rev. Mater.* **2018**, *3*, 143.
[25] R. Nasseri, N. Bouzari, J. Huang, H. Golzar, S. Jankhani, X. (Shirley) Tang, T. H. Mekonnen, A. Aghakhani, H. Shahsavan, *Nat. Commun.* **2023**, *14*, 6108.
[26] X. Deng, M. Korogiannaki, B. Rastegari, J. Zhang, M. Chen, Q. Fu, H. Sheardown, C. D. M. Filipe, T. Hoare, *ACS Appl. Mater. Interfaces* **2016**, *8*, 22064.
[27] D. Kang, J. I. Lee, B. Maeng, S. Lee, Y. Kwon, M. S. Kang, J. Park, J. Kim, *ACS Nano* **2022**, *16*, 15827.
[28] S. O. Blacklow, J. Li, B. R. Freedman, M. Zeidi, C. Chen, D. J. Mooney, *Sci. Adv.* **2019**, *5*, eaaw3963.
[29] M. Kuddushi, X. Deng, J. Nayak, S. Zhu, B. B. Xu, X. Zhang, *ACS Appl. Bio Mater.* **2023**, *6*, 3810.
[30] P. Rao, T. L. Sun, L. Chen, R. Takahashi, G. Shinohara, H. Guo, D. R. King, T. Kurokawa, J. P. Gong, *Adv. Mater.* **2018**, *30*, 1801884.
[31] Y. Jiang, X. Zhang, W. Zhang, M. Wang, L. Yan, K. Wang, L. Han, X. Lu, *ACS Nano* **2022**, *16*, 8662.
[32] Y. He, Q. Li, P. Chen, Q. Duan, J. Zhan, X. Cai, L. Wang, H. Hou, X. Qiu, *Nat. Commun.* **2022**, *13*, 7666.
[33] J. J. Kearney, J. M. Lahey, S. Borirakchanyavat, D. M. Schwartz, D. Wilson, S. C. Tanaka, D. Robins, *Am. J. Ophthalmol.* **2004**, *137*, 96.
[34] M. Guicherd, M. B. Khaled, M. Guéroult, J. Nomme, M. Dalibey, F. Grimaud, P. Alvarez, E. Kamionka, S. Gavalda, M. Noël, M. Vuillemin, E. Amillastre, D. Labourdette, G. Cioci, V. Tournier, V. Kitpreechavanich, P. Dubois, I. André, S. Duquesne, A. Marty, *Nature* **2024**, *631*, 884.
[35] Q. Huang, M. Hiyama, T. Kabe, S. Kimura, T. Iwata, *Biomacromolecules* **2020**, *21*, 3301.
[36] J. Hu, G. Zhang, S. Liu, *Chem. Soc. Rev.* **2012**, *41*, 5933.
[37] S. R. Goudu, I. C. Yasa, X. Hu, H. Ceylan, W. Hu, M. Sitti, *Adv. Funct. Mater.* **2020**, *30*, 2004975.
[38] B. D. Ulery, L. S. Nair, C. T. Laurencin, *J. Polym. Sci. Part B: Polym. Phys.* **2011**, *49*, 832.
[39] B. R. Freedman, O. Uzun, N. M. M. Luna, A. Rock, C. Clifford, E. Stoler, G. Östlund-Sholars, C. Johnson, D. J. Mooney, *Adv. Mater.* **2021**, *33*, 2008553.
[40] J. A. Burdick, G. D. Prestwich, *Adv. Mater.* **2011**, *23*, H41.
[41] W. B. Han, J. H. Lee, J. Shin, S. Hwang, *Adv. Mater.* **2020**, *32*, 2002211.
[42] M. Zhang, C.-C. Song, F.-S. Du, Z.-C. Li, *ACS Appl. Mater. Interfaces* **2017**, *9*, 25905.
[43] C. Li, C. Guo, V. Fitzpatrick, A. Ibrahim, M. J. Zwierstra, P. Hanna, A. Lechtig, A. Nazarian, S. J. Lin, D. L. Kaplan, *Nat. Rev. Mater.* **2020**, *5*, 61.
[44] N. Ashammakhi, A. L. Hernandez, B. D. Unluturk, S. A. Quintero, N. R. de Barros, E. H. Apu, A. B. Shams, S. Ostrovidov, J. Li, C. Contag, A. S. Gomes, M. Holgado, *Adv. Funct. Mater.* **2021**, *31*, 2104149.
[45] L. E. Freed, G. C. Engelmayr, J. T. Borenstein, F. T. Moutos, F. Guilak, *Adv. Mater.* **2009**, *21*, 3410.
[46] X. Yuan, W. Zhu, Z. Yang, N. He, F. Chen, X. Han, K. Zhou, *Adv. Mater.* **2024**, *36*, 2403641.
[47] L. Zhu, T. Yu, W. Wang, T. Xu, W. Geng, N. Li, X. Zan, *Adv. Mater.* **2024**, *36*, 2308728.
[48] O. S. Fenton, K. N. Olafson, P. S. Pillai, M. J. Mitchell, R. Langer, *Adv. Mater.* **2018**, *30*, 1705328.
[49] M. K. Gupta, J. R. Martin, B. R. Dollinger, M. E. Hattaway, C. L. Duvall, *Adv. Funct. Mater.* **2017**, *27*.
[50] C. J. Higginson, S. Y. Kim, M. Peláez-Fernández, A. Fernández-Nieves, M. G. Finn, *J. Am. Chem. Soc.* **2015**, *137*, 4984.
[51] L. Fu, X. Sui, A. E. Crolais, W. R. Gutekunst, *Angew. Chem., Int. Ed.* **2019**, *58*, 15726.
[52] K. Hu, J. Sun, Z. Guo, P. Wang, Q. Chen, M. Ma, N. Gu, *Adv. Mater.* **2015**, *27*, 2507.
[53] F. Gao, H. Jiang, D. Wang, S. Wang, W. Song, *Adv. Mater.* **2024**, *36*, 2401645.
[54] J. Liu, Y. Pang, S. Zhang, C. Cleveland, X. Yin, L. Booth, J. Lin, Y.-A. L. Lee, H. Mazdiyasni, S. Saxton, A. R. Kirtane, T. von Erlach, J. Rogner, R. Langer, G. Traverso, *Nat. Commun.* **2017**, *8*, 124.
[55] R. G. Fonseca, F. D. Bon, P. Pereira, F. M. Carvalho, M. Freitas, M. Tavakoli, A. C. Serra, A. C. Fonseca, J. F. J. Coelho, *Mater. Today Bio* **2022**, *15*, 100325.
[56] A. Herrmann, R. Haag, U. Schedler, *Adv. Healthcare Mater.* **2021**, *10*, 2100062.
[57] C. Zhang, Q. Xie, R. Cha, L. Ding, L. Jia, L. Mou, S. Cheng, N. Wang, Z. Li, Y. Sun, C. Cui, Y. Zhang, Y. Zhang, F. Zhou, X. Jiang, *Adv. Healthcare Mater.* **2021**, *10*, 2100839.
[58] S. Dimitrievska, J. Wang, T. Lin, A. Weyers, H. Bai, L. Qin, G. Li, C. Cai, A. Kypson, N. Kristofik, A. Gard, S. Sundaram, K. Yamamoto, W. Wu, L. Zhao, M. H. Kural, Y. Yuan, J. Madri, T. R. Kyriakides, R. J. Linhardt, L. E. Niklason, *Adv. Funct. Mater.* **2020**, *30*, 1908963.
[59] R. Raman, T. Hua, D. Gwynne, J. Collins, S. Tamang, J. Zhou, T. Esfandiary, V. Soares, S. Pajovic, A. Hayward, R. Langer, G. Traverso, *Sci. Adv.* **2020**, *6*, eaay0065.
[60] R. G. Fonseca, A. Kuster, P. P. Fernandes, M. Tavakoli, P. Pereira, J. R. Fernandes, F. D. Bon, A. C. Serra, A. C. Fonseca, J. F. J. Coelho, *Adv. Healthcare Mater.* **2023**, *12*, 2300918.
[61] D. Kang, J. Kim, *J. Am. Chem. Soc.* **2021**, *143*, 5616.
[62] D. Kang, S. Lee, J. Kim, *Chem* **2022**, *8*, 2260.
[63] M. Kobašlija, D. T. McQuade, *Biomacromolecules* **2006**, *7*, 2357.
[64] D. Kang, S. T. Cheung, J. Kim, *Angew. Chem., Int. Ed.* **2021**, *60*, 16947.

[65] D. Kang, S. T. Cheung, A. Wong-Rolle, J. Kim, *ACS Cent. Sci.* **2021**, *7*, 631.
[66] R. S. Rivlin, A. G. Thomas, *J. Polym. Sci.* **1953**, *10*, 291.
[67] E. Mariner, S. L. Haag, M. T. Bernards, *Biointerphases* **2019**, *14*, 031002.
[68] M.-J. Xie, C.-C. Wang, R. Zhang, J. Cao, M.-Z. Tang, Y.-X. Xu, *Polymer* **2024**, *290*, 126550.
[69] J. A. Cintron-Cruz, B. R. Freedman, M. Lee, C. Johnson, H. Ijaz, D. J. Mooney, *Adv. Mater.* **2022**, *34*, 2205567.
[70] B. R. Freedman, J. A. C. Cruz, P. Kwon, M. Lee, H. M. Jeffers, D. Kent, K. C. Wu, J. C. Weaver, D. J. Mooney, *Proc. Natl. Acad. Sci.* **2024**, *121*, 2304643121.
[71] H. Yang, C. Li, J. Tang, Z. Suo, *ACS Appl. Bio Mater.* **2019**, *2*, 1781.
[72] X. Ni, Z. Yang, J. Li, *ACS Macro Lett.* **2021**, *10*, 180.
[73] R. P. Dumitriu, A. Oprea, C. N. Cheaburu, M. Nistor, O. Novac, C. M. Ghiciuc, L. Profire, C. Vasile, *J. Appl. Polym. Sci.* **2014**, *131*, 40733.
[74] R. P. Dumitriu, A. M. Oprea, C. Vasile, *Solid State Phenom.* **2009**, *154*, 17.
[75] H. Zhang, Y. Zhang, L. He, B. Yang, S. Zhu, M. Yao, *Colloid Polym. Sci.* **2016**, *294*, 1959.
[76] H. K. Ju, S. Y. Kim, S. J. Kim, Y. M. Lee, *J. Appl. Polym. Sci.* **2002**, *83*, 1128.
[77] W. J. Zheng, N. An, J. H. Yang, J. Zhou, Y. M. Chen, *ACS Appl. Mater. Interfaces* **2015**, *7*, 1758.
[78] J. Wu, Z. Pan, Z. Zhao, M. Wang, L. Dong, H. Gao, C. Liu, P. Zhou, L. Chen, C. Shi, Z. Zhang, C. Yang, S. Yu, D. Zou, *Adv. Mater.* **2022**, *34*, 2200115.
[79] Y. Ding, Z. Zhu, X. Zhang, J. Wang, *Adv. Healthcare Mater.* **2024**, *23*, 2400912.
[80] M. Y. Gorshkova, L. V. Vanchugova, I. F. Volkova, I. V. Obydennova, I. L. Valuev, L. I. Valuev, *Mendeleev Commun.* **2022**, *32*, 189.
[81] W. Zhang, B. Bao, F. Jiang, Y. Zhang, R. Zhou, Y. Lu, S. Lin, Q. Lin, X. Jiang, L. Zhu, *Adv. Mater.* **2021**, *33*, 2105667.
[82] K. Matsumoto, N. Sakikawa, T. Miyata, *Nat. Commun.* **2018**, *9*, 2315.
[83] S. Lanzalaco, J. Mingot, J. Torras, C. Alemán, E. Armelin, *Adv. Eng. Mater.* **2023**, *25*, 2201303.
[84] D. T. Wu, B. R. Freedman, K. H. Vining, D. L. Cuylear, F. P. S. Guastaldi, Y. Levin, D. J. Mooney, *J. Dent. Res.* **2023**, *102*, 497.
[85] B. Marco-Dufort, J. R. Janczy, T. Hu, M. Lütolf, F. Gatti, M. Wolf, A. Woods, S. Tetter, B. V. Sridhar, M. W. Tibbitt, *Sci. Adv.* **2022**, *8*, eabo0502.
[86] H. Keum, E. Cevik, J. Kim, Y. M. Demirlenk, D. Atar, G. Saini, R. A. Sheth, A. R. Deipolyi, R. Oklu, *Adv. Mater.* **2024**, *36*, 2310856.